Earth, Planets and Space

FULL PAPER

Open Access

Reconstruction of a phreatic eruption on 27 September 2014 at Ontake volcano, central Japan, based on proximal pyroclastic density current and fallout deposits

Fukashi Maeno[1*], Setsuya Nakada[1], Teruki Oikawa[2], Mitsuhiro Yoshimoto[3], Jiro Komori[4], Yoshihiro Ishizuka[2], Yoshihiro Takeshita[5], Taketo Shimano[6], Takayuki Kaneko[1] and Masashi Nagai[7]

Abstract

The phreatic eruption at Ontake volcano on 27 September 2014, which caused the worst volcanic disaster in the past half-century in Japan, was reconstructed based on observations of the proximal pyroclastic density current (PDC) and fallout deposits. Witness observations were also used to clarify the eruption process. The deposits are divided into three major depositional units (Units A, B, and C) which are characterized by massive, extremely poorly sorted, and multimodal grain-size distribution with 30–50 wt% of fine ash (silt–clay component). The depositional condition was initially dry but eventually changed to wet. Unit A originated from gravity-driven turbulent PDCs in the relatively dry, vent-opening phase. Unit B was then produced mainly by fallout from a vigorous moist plume during vent development. Unit C was derived from wet ash fall in the declining stage. Ballistic ejecta continuously occurred during vent opening and development. As observed in the finest population of the grain-size distribution, aggregate particles were formed throughout the eruption, and the effect of water in the plume on the aggregation increased with time and distance. Based on the deposit thickness, duration, and grain-size data, and by applying a scaling analysis using a depth-averaged model of turbulent gravity currents, the particle concentration and initial flow speed of the PDC at the summit area were estimated as 2×10^{-4}–2×10^{-3} and 24–28 m/s, respectively. The tephra thinning trend in the proximal area shows a steeper slope than in similar-sized magmatic eruptions, indicating a large tephra volume deposited over a short distance owing to the wet dispersal conditions. The Ontake eruption provided an opportunity to examine the deposits from a phreatic eruption with a complex eruption sequence that reflects the effect of external water on the eruption dynamics.

Keywords: Phreatic eruption, Pyroclastic density current, Ontake volcano, Aggregate, Grain-size distribution, Particle concentration, Flow speed

Background

Volcanic eruptions can violently expel only non-juvenile materials. Such eruptions are caused by catastrophic failure of country rock owing to pressurization of the gas–fluid sources or flashing of superheated water at shallow levels (e.g., Wohletz and Heiken 1992). The eruptions are

often called 'phreatic' eruptions, implying that heated groundwater is a major driving force in the expulsion of the country rock, or a 'hydrothermal' eruption, if fluid from a hydrothermal system is involved (e.g., Hedenquist and Henley 1985; Mastin 1995). Heating by ascending fresh magma can also trigger eruptions of non-juvenile material as seen in precursor events of magmatic eruptions (e.g., Barberi et al. 1992; Young et al. 1998; Suzuki et al. 2013). Phreatic eruptions tend to be of smaller scale in terms of the volume of the products, and the

*Correspondence: fmaeno@eri.u-tokyo.ac.jp
[1] Earthquake Research Institute, The University of Tokyo, 1-1-1, Yayoi, Bunkyo-ku, Tokyo 113-0032, Japan
Full list of author information is available at the end of the article

Maeno *et al. Earth, Planets and Space* (2016) 68:82

Page 2 of 20

temperature of the ejected material (a few 100 °C) is generally much lower than that of magmatic eruptions (Feuillard et al. 1983; Hedenquist and Henley 1985; Barberi et al. 1992; Browne and Lawless 2001). However, non-juvenile eruptions are not necessarily less disastrous; rather, they are more likely to cause damage than magmatic eruptions in some situations. They are occasionally very intense and often occur without clear precursor signals. They can also last a relatively long period (e.g., ~8 months for the La Soufrière event, Guadeloupe, in 1975–1976), resulting in a difficult scenario that requires managing a complex eruption sequence (Feuillard et al. 1983; Hincks et al. 2014). Moreover, non-magmatic eruptions sometimes lead to partial edifice collapse and laterally directed violent explosions (e.g., Bandai, Japan; Tongariro, NZ; La Soufrière, Guadeloupe).

The eruption at Ontake volcano on 27 September 2014 was the worst volcanic disaster (58 deaths and five missing persons) in Japan in the past half-century; many of the casualties were climbers who were close to the summit of the mountain at the time of the eruption. Reconstruction of phreatic events based on geological and witness records is important to understand the nature of these eruptions and to evaluate potential hazards related to phreatic eruptions. However, such studies are limited to relatively large-scale past phreatic events (e.g., Bandai volcano, Yamamoto et al. 1999; Adatara volcano, Fujinawa et al. 2008) and recent well-observed eruptions (e.g., Heiken et al. 1980; Ohba et al. 2007; Lube et al. 2014), and there are still uncertainties on quantitative estimation of the eruption processes based on geological records. The eruption at Ontake volcano provides an opportunity to study the process of a phreatic eruption. In this paper, we characterize the proximal pyroclastic density currents (PDCs) and fallout deposits of this eruption. We reconstruct the eruption process and estimate the physical parameters (volume, velocity, and particle concentration) of the associated PDCs based on geological and witness records and apply a scaling analysis using a depth-averaged model of gravity currents flowing down slopes.

Methods

First, we overview the eruption at Ontake volcano on 27 September 2014, based on direct observations by monitoring instruments and witnesses. Then, we present geological data obtained by our field surveys at proximal and distal sites. The distribution, thickness, and description of the tephra deposit are presented. The data were used to estimate the physical parameters of the eruption such as tephra volume. We also present laboratory analysis of the grain-size characteristics of the deposit using the mechanical sieving method and laser diffraction

particle-size analyzer, and component analysis by microscope and X-ray powder diffractometer (XRD). Based on the geological and witness records and the laboratory data, we discuss the eruption process.

Outline of the eruption

Ontake volcano is one of the highest active volcanoes in Japan, with a summit elevation of 3067 m above sea level (a.s.l.) at Kengamine Peak (Fig. 1). Recent volcanic activity includes the phreatic eruptions of 1979, 1991, and 2007, and fumarolic activity at the Jigokudani area that lasted at least a few 100 years (Oikawa 2008). The phreatic eruption in 1979 was the first historically recorded explosion event at Ontake volcano and was on a similar scale to the 2014 eruption in terms of volume and tephra distribution (Kobayashi 1980). The phreatic eruptions in 1991 and 2007 that were much smaller than the 1979 and 2014 eruptions generated only minor ash plumes and caused no casualties (Japan Meteorological Agency 1991; Nakamichi et al. 2009). These recent eruptions and associated seismic activities such as very long-period (VLP) events indicate that a shallow hydrothermal system heated by an intruded magma is developing beneath Ontake volcano (Nakamichi et al. 2009). At Ontake, a seismic swarm occurred during 10–11 September 2014 and the Japan Meteorological Agency (JMA) issued a Volcanic Information notice that included a warning to the towns situated around the volcano of a possible small phreatic eruption. However, the seismicity declined over the following days, with only a few low-frequency seismic events recorded during 11–27 September. A later seismological study revealed that the frequency of volcano tectonic (VT) earthquakes gradually increased from 6 September 2014 and reached a peak on 11 September 2014, and then seismicity levels remained elevated until the eruption (Kato et al. 2015).

The eruption began at 11:52 (local time, used hereafter) on 27 September with vigorous ash emission from the Jigokudani area at an altitude of around 2700–2750 m a.s.l., about 500 m from Kengamine Peak. Immediately before the eruption, volcanic tremor and tilt changes were recorded at 11:41 and 11:45, respectively, at the JMA stations at Tanohara, 2 km SE of the summit (Japan Meteorological Agency 2014). The migration of VT earthquakes in the up-dip direction during the last 10 min before the eruption, which coincided with tremor and tilt changes, suggests that the vertical conduit was filled with pressurized fluids that rapidly propagated to the surface (Kato et al. 2015). These geophysical records are thought to be precursor phenomena of the eruption, although it was not possible to issue alerts before the eruption based on these phenomena. The eruption was confirmed at 11:52 by seismic and tilt records at the
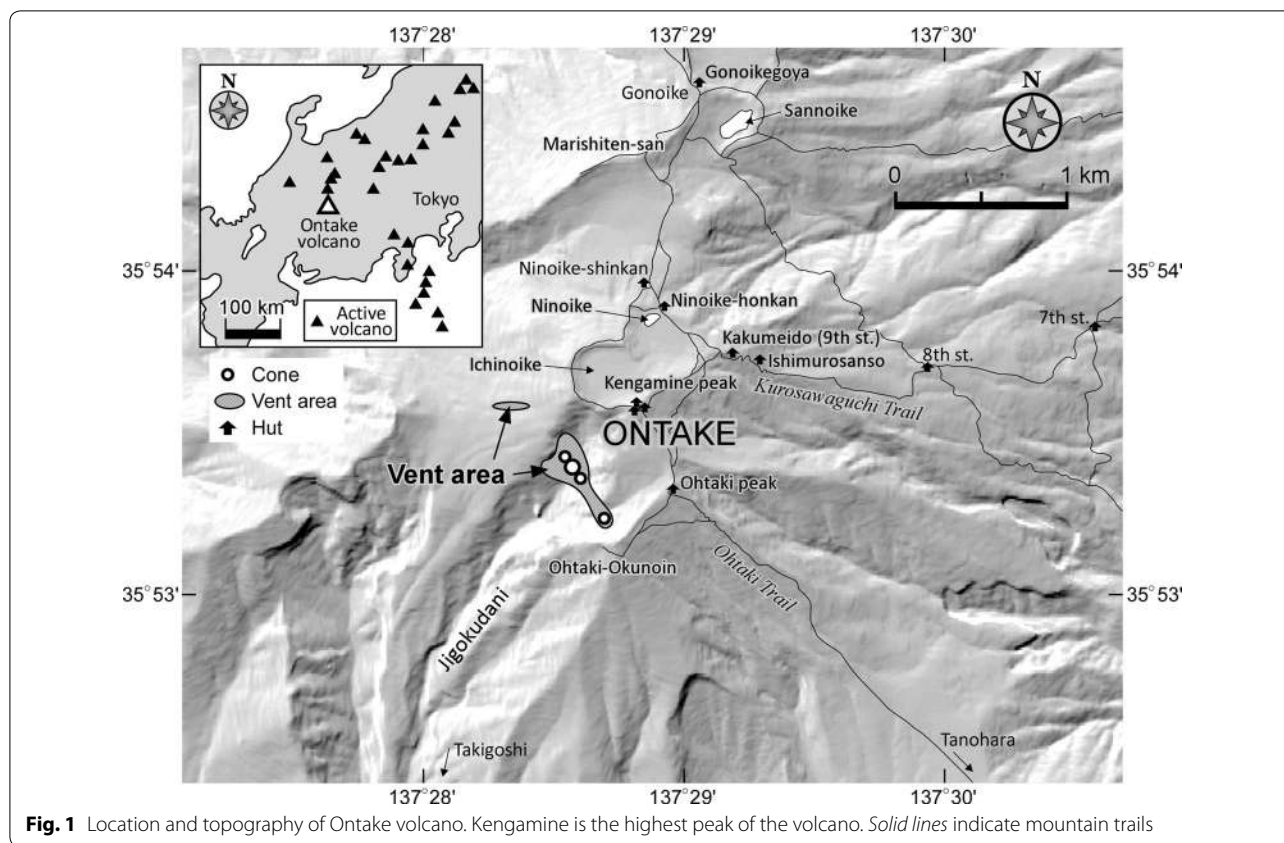
Maeno *et al. Earth, Planets and Space* (2016) 68:82

Page 3 of 20

Fig. 1 Location and topography of Ontake volcano. Kengamine is the highest peak of the volcano. *Solid lines* indicate mountain trails

Tanohara station (Japan Meteorological Agency 2014). At the same time, climbers around the summit area witnessed an ash cloud rapidly rising from the Jigokudani valley and then a growing ash cloud covering the summit with a shower of ballistic ejecta.

Major PDCs travelled down the southern slope (Jigokudani valley) and the western slope of the Ichinoike cone. They were recorded by a video camera operated by the Chubu Regional Bureau, Ministry of Land, Infrastructure, Transport and Tourism, at Takigoshi about 6 km SSW of the summit. The most extensive PDC travelled for about 2.4 km along the Jigokudani valley between 11:53 and 11:59. The PDC generated a buoyant liftoff cloud caused by elutriation of fine ash particles during the final stage of emplacement. According to photographs and video images taken by climbers at the eastern and northern slopes, other PDCs also occurred when an eruption plume collapsed, covering the summit area. From Ninoike, at the northern side of the summit, Mr. Kodera, a staff member at the climbers' hut (Ninoike-Honkan), took sequential photographs of the eruption plume and the PDCs developing from the foot of the rising plume, indicating fountain collapse (Fig. 2). In the first photograph (11:53:40, the time was estimated based on other photographs, video images, and interviews, Oikawa et al.

2016), the summit area and Ichinoike are being covered by a PDC ash cloud. The photograph also shows a number of ballistic ejecta preceding the PDCs, hitting the ground, and producing impact dust. A lobe of PDC (right-hand side of the photograph at 11:53:40) is slowly moving toward the north (11:54:30). The whitish ash layer was formed from the body of the PDC ash cloud between 11:54:30 and 11:54:48. The lobe rose because of deposition and elutriation of the fine ash, resulting in the formation of a buoyancy co-PDC liftoff cloud (11:54:48). It remained behind the peak until the PDCs completely covered the summit area (11:55:52). After that, a new lobe of PDC emerged from a topographic depression, advanced toward Ninoike, and formed the deposit (11:56:14). The flow then stopped and the ash cloud accompanying the PDC began to rise (11:56:58). The light-gray-colored, thin PDC deposit can be clearly identified in the photographs taken at 11:55:52 (Fig. 3a) and 11:56:58 (Fig. 3b). These sequential photographs show that the PDC event was preceded by ballistic ejecta and was not a single event but a sequence of bursts. The ash layer seems thin, probably less than a few cm; this is consistent with field observation around this area as described later.
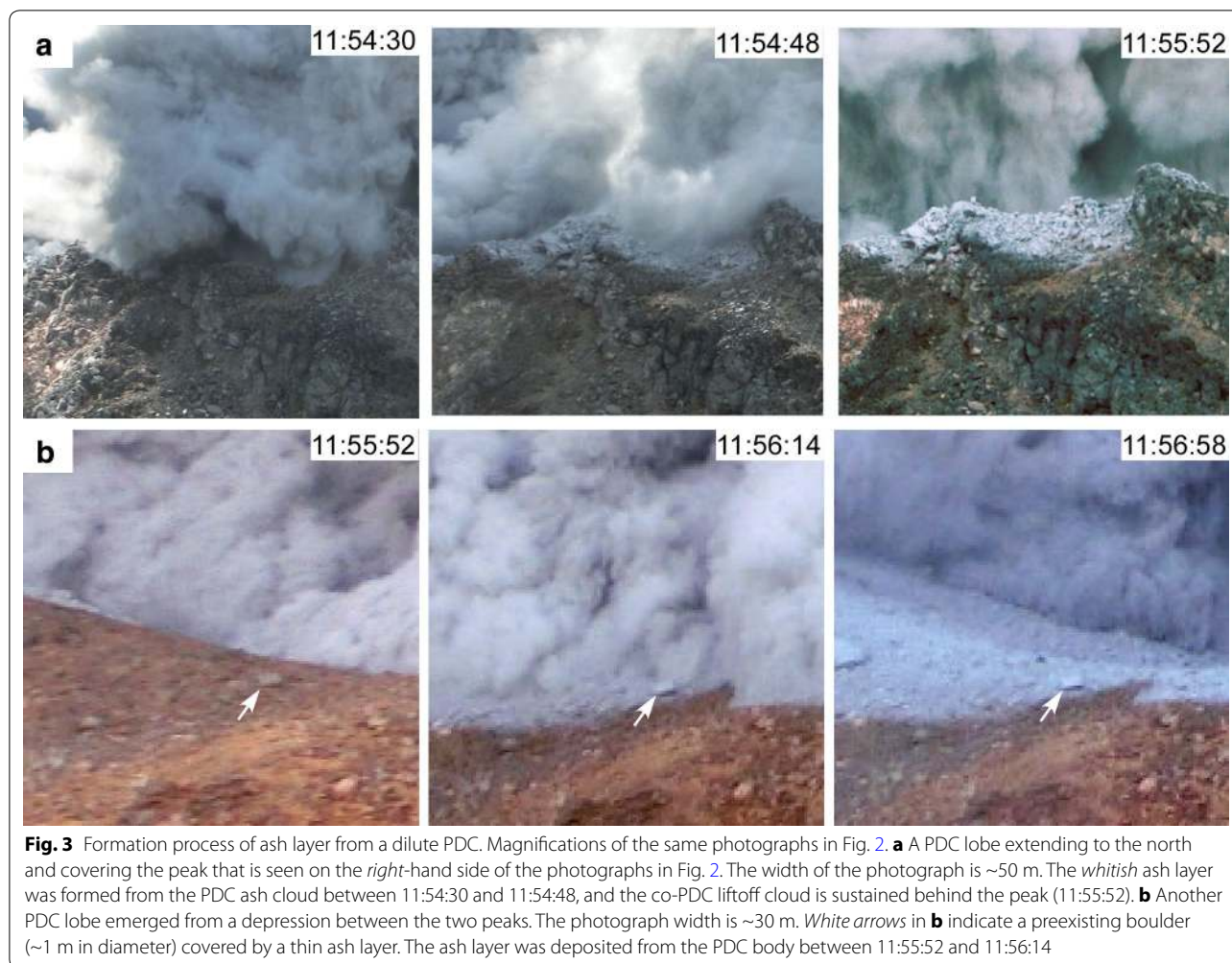
According to interviews with climbers who stayed in and around the huts at the summit area [e.g., from The

Maeno *et al. Earth, Planets and Space* (2016) 68:82

Page 4 of 20

Fig. 2 Photographs showing the development of the plume and PDCs in the initial phase of the Ontake eruption. The distance between the two peaks is about 300 m. The height of the peak to the *right* of Ninoike pond is about 100 m. Photographs taken by Mr. Y. Kodera from Ninoike-Honkan

Shinano Mainichi Shimbun (2015)], the eruption cloud began to rise with no discernible sounds. After the emergence of the eruption cloud, some people heard a loud noise repeatedly from the direction of Jigokudani, followed by the development of the eruption cloud. As the ash cloud covered the sky, it grew dark; in the darkness, which lasted 20–30 min, climbers and staff who found shelter in the huts heard noises caused by sandy material

and blocks hitting the roofs, walls, and windows of the buildings violently and intermittently. After 30 min, it became light for a short time and then darkened again. The interview reports suggest that the eruption event was dominated by intermittent, vigorous fallout or PDCs and ballistic ejecta in the proximal area and that the deposition of most of the eruptive material lasted at least half an hour. Oikawa et al. (2016) suggested that the

Maeno *et al. Earth, Planets and Space* (2016) 68:82

Page 5 of 20

Fig. 3 Formation process of ash layer from a dilute PDC. Magnifications of the same photographs in Fig. 2. **a** A PDC lobe extending to the north and covering the peak that is seen on the *right*-hand side of the photographs in Fig. 2. The width of the photograph is ~50 m. The *whitish* ash layer was formed from the PDC ash cloud between 11:54:30 and 11:54:48, and the co-PDC liftoff cloud is sustained behind the peak (11:55:52). **b** Another PDC lobe emerged from a depression between the two peaks. The photograph width is ~30 m. *White arrows* in **b** indicate a preexisting boulder (~1 m in diameter) covered by a thin ash layer. The ash layer was deposited from the PDC body between 11:55:52 and 11:56:14

temperature of the PDCs partially exceeded 100 °C but was mostly in the range 30–100 °C, based on an analysis of the interview reports. Most of the injures and deaths that occurred in this eruption are thought to have been caused by ballistic blocks with high velocity, hence high landing energy (Tsunematsu et al. 2016), that continued to land throughout most of the eruption period, rather than by low-temperature, dilute PDCs that mainly occurred in the initial phase of the eruption.

Sato et al. (2015) reported that the plume height eventually increased and reached about 10,000 m a.s.l. at 12:10, based on analyses of Doppler radar data. Therefore, when the photographs of the PDCs were taken from Ninoike-Honkan, the main eruption plume had just developed. The plume height then decreased to 7000 m a.s.l. at 12:20 and reached 4000–5000 m a.s.l. by 18:00 (Sato et al. 2015). The direct observations and the plume height data suggest that multiple PDCs were generated at the summit area by partial collapse of the growing eruption plume. Ash fall was observed mainly at the eastern

side of the volcano. The tephra dispersal area extended to at least ~80 km from the summit. The ash-fall deposit is thought to have developed from a direct plume and a co-PDC plume. In the source area of the Jigokudani valley, at least three pyroclastic cones formed within about 3 h after the onset of the eruption in the vent area, trending NW–SE. One of these cones is thought to have been the main source of the initial eruption phase (the largest circle in the vent area in Fig. 1), and the others were formed at least 2–3 h after the initial eruption, based on analyses of aerial photographs (Kaneko et al. 2016). Aerial photographs indicate that the diameter of each crater is several tens of meters and the average height of the vent area is a few to 10 m. Mudflows emerged from some of the cones and flowed down the Jigokudani valley. Wet products characterize the later phase of the eruption, as indicated by sun cracks that developed on the deposit surface and by the residual water at the bottom of impact craters observed during a helicopter survey on the day following the eruption (Kaneko et al. 2016). However, there is no

Maeno *et al. Earth, Planets and Space* (2016) 68:82

Page 6 of 20

evidence of wet deposition in the proximal area during the initial phase (Oikawa et al. 2016). Thus, the eruption started in a relatively dry state and eventually changed to wet conditions.

Results

Distribution and thickness of the eruptive deposits

The eruptive deposits on the edifice of the Ontake volcano were investigated along trails on the SE side (Ohtaki Trail), the NE side (Kurosawaguchi Trail), the N side (Ninoike–Gonoike Trail), and the summit area (Figs. 1, 4). The preliminarily report of Oikawa et al. (2015) showed that the total thickness of the deposits generally decreases with distance from the vent area, although it varies depending on the topography; the thicker deposits (30–70 cm) are distributed around Kengamine Peak. Ohtaki Peak, SE of the vent area, is close to the vent, but the deposit there is <10 cm thick. At the NE side near Kakumeido (9th station), 1 km from the vent area, the maximum deposit thickness is 12 cm. In the area ~3 km from the summit, the thickness of the deposit decreases to <1 cm.

The deposits around the summit area include not only fallout tephra but also PDC deposits (Fig. 4a). The distribution of the PDC deposits on the southern and western slopes was determined based on aerial photographs taken by the Geospatial Information Authority of Japan (GSI) (2014) and Kaneko et al. (2016). The major PDC deposits extend 1.5 km and 2.4 km from the vent in the NW and SW directions, respectively. Although it is difficult to determine the distribution of the PDC deposits in the northern and eastern sides based only on aerial photographs, geological and witness observations suggest that the PDC deposits also extend ~1 km or more from the vent on the NE and E sides. The distribution of the PDC deposits in this direction is a little narrower than the distribution of the PDCs determined based only on witness observations (Oikawa et al. 2016). The discrepancy may be owing to difficulty in determining the distal limit of the PDC deposits. Additionally, the dispersal axis of the fallout tephra extending ENE makes it difficult to distinguish between the fallout and the flow deposits in this direction. The thickness estimation may be close to the minimum value, because our surveys at the summit area were carried out more than 1 month after the eruption. Therefore, erosion and disturbance caused by the reworking process and searching operations for missing persons affected the original deposit structures at many locations. During the field survey, we carefully selected sites where the primary tephra deposits were preserved.

Distal ash fall from the Ontake eruption was observed at many locations in the eastern side of the volcano in the afternoon of 27 September 2014. The Joint Research Team for Ash Fall from the Ontake 2014 Eruption (2015) surveyed the distribution of ash-fall deposit and produced the isomass contour map (Fig. 4c). The 1 g/m^2 contour extends ~80 km to the east. The isomass contours suggest that the eruption plume was primarily affected by a strong seasonal westerly wind, though minor ash fall was observed at the western side of the volcano.

Eruption deposit facies

The eruption deposits consist of three major units (Units A, B, and C) in the proximal area. Here, we define 'proximal' as the summit area within 0.5–1.0 km from the vent area, corresponding approximately to the 8-cm thickness contour (Fig. 4b). The representative outcrop locations (*a*)–(*k*) and the topographic relationship in the proximal area are shown in Fig. 5. The entire deposit sequence is 5–70 cm thick and overlies the pre-eruption, orange-colored ground surface (Fig. 6). All the outcrops occur in areas that are 200–300 m higher than the vent area. At some locations, one of the units is missing or indistinguishable from the other units. Column sections of representative locations are shown in Fig. 7.

Unit A consists of the lowest part of the deposit and is 1–5 cm thick (Fig. 4a), overlying the pre-eruption ground surface without erosion signatures. Generally, the thickness decreases with distance from the vent but is thicker in topographic depressions at some locations. The deposited material is gray, massive, and poorly sorted, with a dominant component of silt- to clay-sized fine ash (see "Grain-size characteristics" section). The unit shows almost no grading structures, but a discontinuous thin ash layer (a few mm thick) composed of sand-sized grains is occasionally embedded [e.g., at location (*b*)]. The distribution of Unit A is limited to the NE–N sides of the vent and is overlaid with a deposit a few tens of cm thick (Unit B). The contact between two units is diffusive. At locations (*d*, *e*), the maximum thickness is ~5 cm. At some locations near the vent area, altered, angular to subangular lava blocks with diameter up to ~10 cm, probably emplaced as ballistic ejecta (fallout) in the initial phase, are also contained in this unit. Unit A corresponds to the thin fine-grained ash layer generated from a PDC body at the initial phase shown in Figs. 2 and 3. The thickness of the deposit from the PDCs shown in the photograph taken from Ninoike (Fig. 3a) was <1 cm as observed around locations (*g*2, *h*).

Unit B consists of the middle layer of the deposits and is generally the thickest one (Fig. 7). The deposit is gray, massive, and poorly sorted, and is coarser than the other units (see also Fig. 8). It consists mainly of silt- to clay-sized fine ash but also contains lapilli- to block-sized altered lava fragments up to 10 cm in diameter (indicated by arrows in the photographs from locations (*g*2,
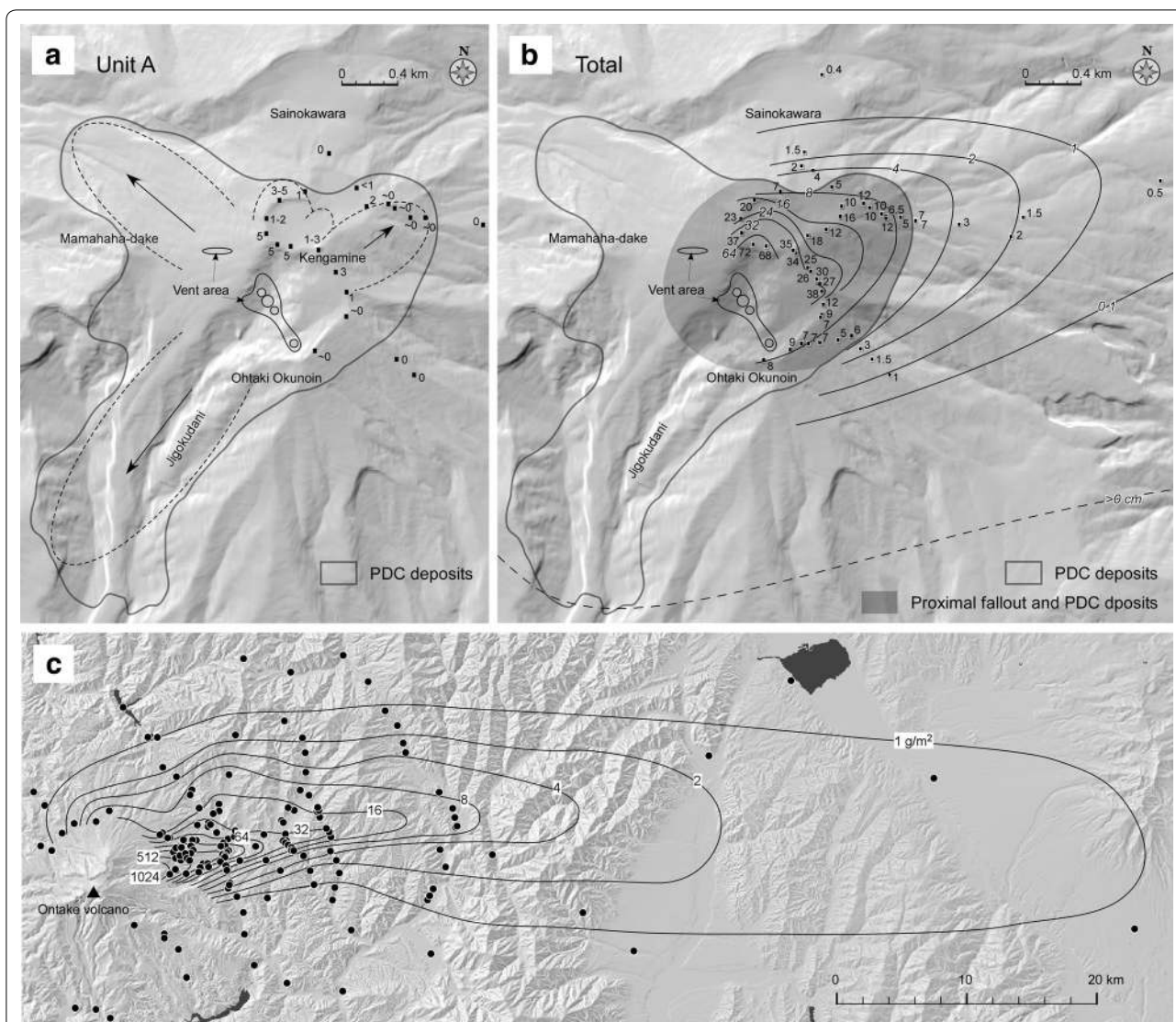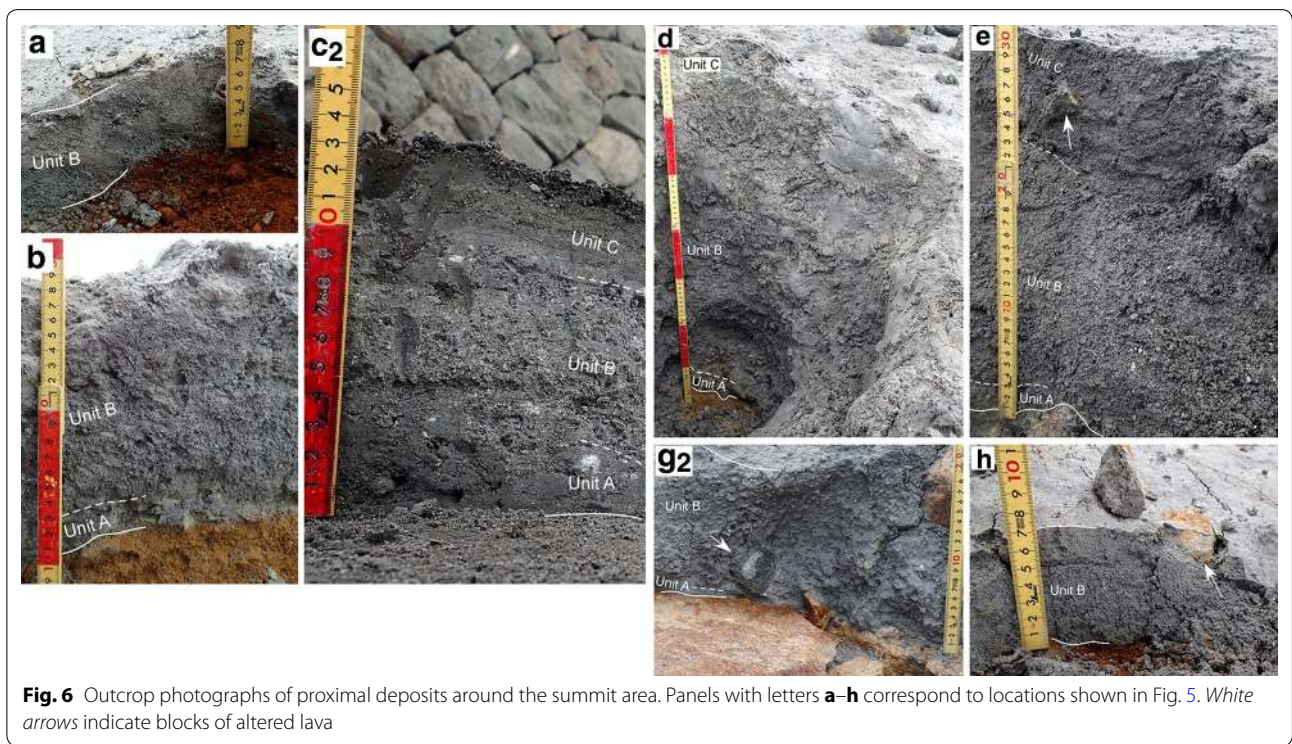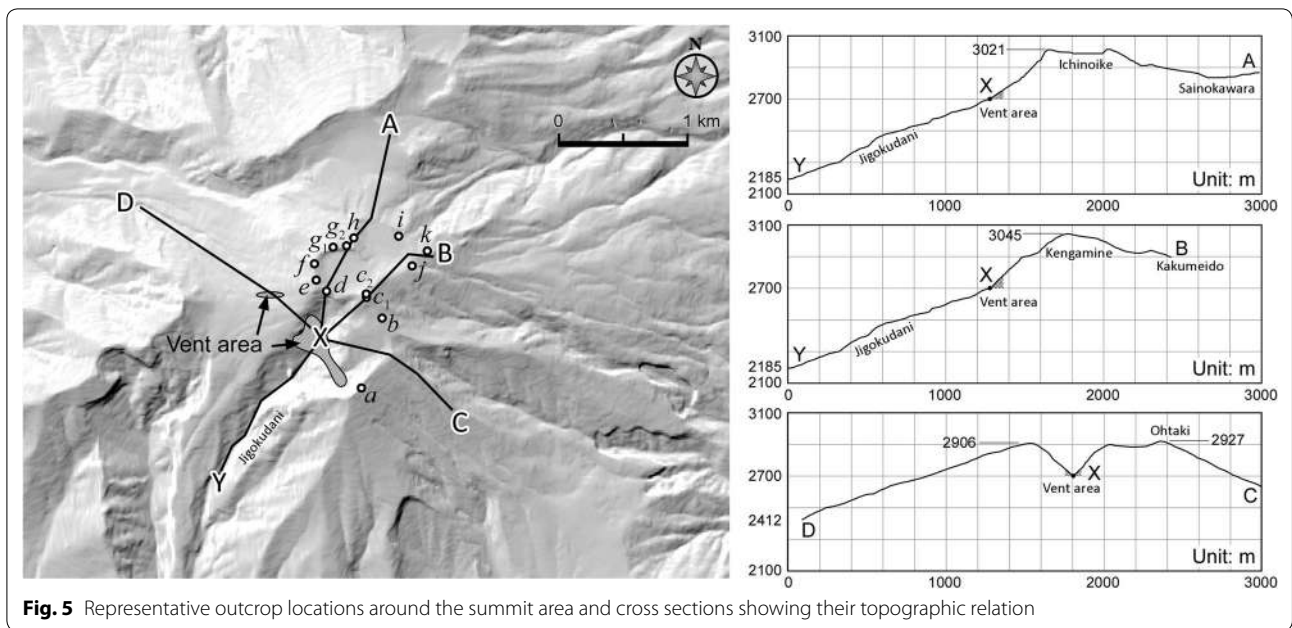
Maeno *et al. Earth, Planets and Space* (2016) 68:82

Page 7 of 20

Fig. 4 **a** Distribution of Unit A (PDC deposits) and thickness data near the summit area (unit is cm). *Broken lines* and *arrows* indicate representative PDC lobes and their directions, respectively. **b** Isopach map of total (fallout and PDC) deposits for the proximal area (unit is cm) and **c** isomass map for the distal area (unit is g/m²). Distal data were provided by—the Joint Research Team for Ash Fall from the Ontake 2014 Eruption (2015)

h) in Fig. 6). The unit is characterized by matrix-supported texture and weak normal and/or reverse grading in the proximal area; however, the grading structure becomes unclear with distance from the vent. Ash accretion textures can be recognized at some locations. The texture is characterized by ash aggregates that have partially coalesced to leave an open void structure, but do not show distinct solid spherical particles. Unit B covers most of the summit area with varying thickness and grain size. The thicker deposits are distributed NE–NW of the Jigokudani area. Most of the eruptive deposit that thickly covered the mountain huts at Kengamine Peak is part of this unit. The deposit in the western side

of Kengamine Peak is particularly thick. The maximum thickness was 72 cm at location (*d*) ~300 m above the vent.

Unit C consists of the uppermost part of the deposit. It is light gray, massive, and poorly sorted. The major components of this unit are silt- to clay-sized fine ash (Fig. 8), and the grain size is finer than that of Units A and B. Ash accretion textures can occasionally be recognized as observed in Unit B. Unit C can be found in various locations throughout the summit area; the layer thickness varies from a few to 10 cm (Fig. 7). Lava blocks with diameter up to ~10 cm, emplaced as ballistic ejecta, are also contained in this unit.
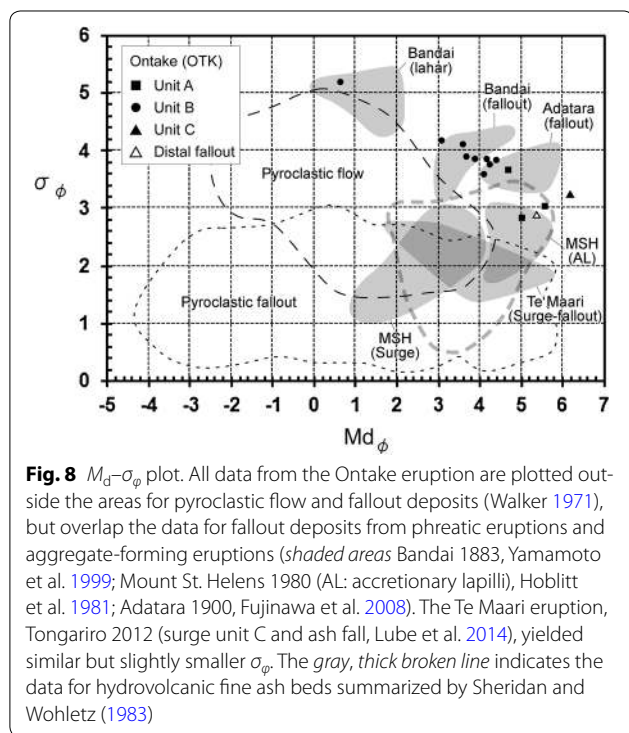
Maeno *et al. Earth, Planets and Space* (2016) 68:82

Page 8 of 20

Fig. 5 Representative outcrop locations around the summit area and cross sections showing their topographic relation

Fig. 6 Outcrop photographs of proximal deposits around the summit area. Panels with letters **a**–**h** correspond to locations shown in Fig. 5. *White arrows* indicate blocks of altered lava
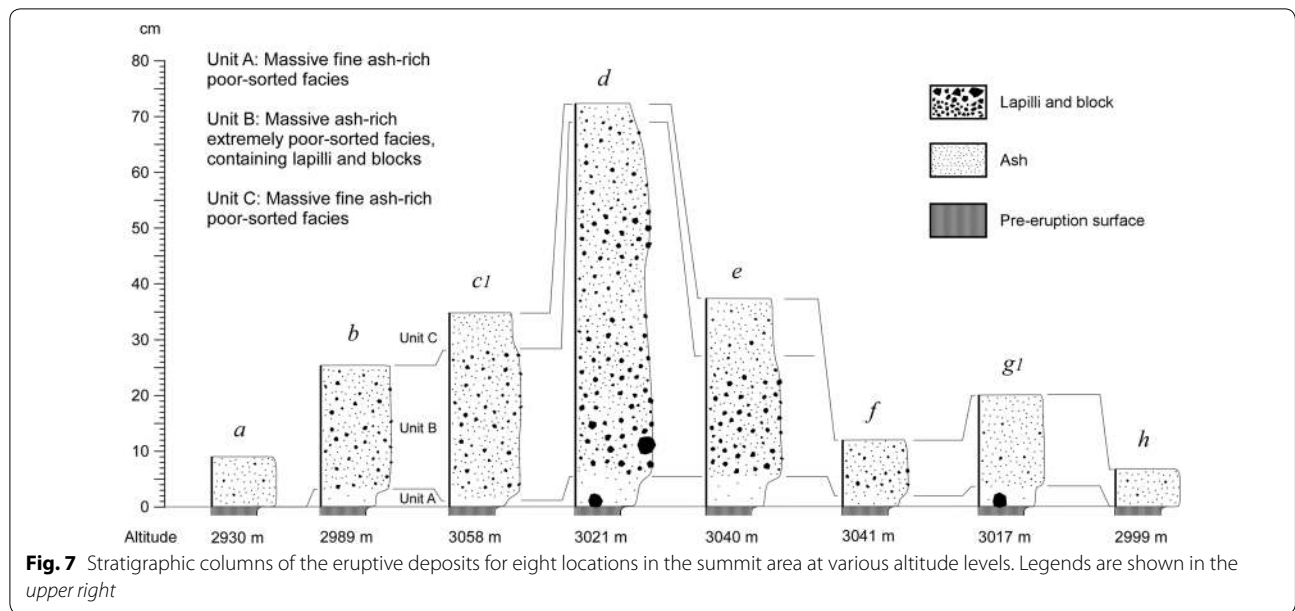
Large lava blocks up to a few tens of cm in diameter were observed on the surface throughout the deposit; some of these large ejecta damaged buildings around the summit area. These blocks were emplaced as ballistic ejecta and are embedded in Unit B and/or C. Immediately after the eruption, numerous impact craters produced by the ballistic ejecta were observed (Kaneko et al. 2016).

Grain-size characteristics

Grain-size analyses were carried out for samples from proximal and distal (6 and 10 km below the dispersal axis)

Maeno *et al. Earth, Planets and Space* (2016) 68:82

Page 9 of 20

Fig. 7 Stratigraphic columns of the eruptive deposits for eight locations in the summit area at various altitude levels. Legends are shown in the *upper right*

Fig. 8 M_d–σ_φ plot. All data from the Ontake eruption are plotted outside the areas for pyroclastic flow and fallout deposits (Walker 1971), but overlap the data for fallout deposits from phreatic eruptions and aggregate-forming eruptions (*shaded areas* Bandai 1883, Yamamoto et al. 1999; Mount St. Helens 1980 (AL: accretionary lapilli), Hoblitt et al. 1981; Adatara 1900, Fujinawa et al. 2008). The Te Maari eruption, Tongariro 2012 (surge unit C and ash fall, Lube et al. 2014), yielded similar but slightly smaller σ_φ. The *gray*, *thick broken line* indicates the data for hydrovolcanic fine ash beds summarized by Sheridan and Wohletz (1983)

particles. Thus, our data represent the entire grain-size distribution. Each sample was first sieved in wet conditions using a $3 - \phi$ sieve. Then, the grain-size distribution for grains coarser than 3ϕ was determined by mechanical sieving at $0.5 - \phi$ intervals. The grains that were finer than 3ϕ were classified by a laser diffraction particle-size analyzer under wet dispersion conditions, using the Sympatec HELOS & RODOS systems (Clausthal-Zellerfeld, Germany). The data obtained from both methods were combined to estimate the entire grain-size distribution assuming the same particle density.

The grain-size histograms for all the samples show widespread size distribution with multiple populations. The Inman parameters (Inman 1952) [the sorting coefficient (σ_ϕ) and median diameter (M_d)] were used to determine the grain-size characteristics. The σ_ϕ of all the samples is within the range 3–5ϕ, indicating extremely poor sorting (Fig. 8). The samples from the distal fallout and the top and bottom positions corresponding to Units A and C in the proximal region are characterized by larger M_d and smaller σ_ϕ values, but are still poorly sorted. The grain characteristics are comparable to representative phreatic and phreatomagmatic eruptions. Most of the samples from Unit B have features similar to those of fallout deposits from the Bandai 1888 eruption (Yamamoto et al. 1999) and the Adatara 1900 eruption (Fujinawa et al. 2008), but show slightly poorer sorting than the deposits from the Te Maari 2012 eruption (Unit C surge and fallout, Lube et al. 2014). One sample is similar to a lahar deposit from the Bandai eruption. However, finer samples such as those from Units A and C and distal fallout deposits show similar characteristics to accretionary lapilli deposits associated with the blast eruption at

locations for the different eruption units. For the proximal locations, the analyses were performed layer by layer. At locations (*d*, *f*), the samples were collected from eight and three stratigraphic levels, respectively. The distal fallout tephra contained aggregate particles; however, it was difficult to analyze the size distribution of the aggregates because they were fragile and the original size could be observed only in the field. Therefore, we analyzed the rough samples of the aggregates that included the fine

Maeno *et al. Earth, Planets and Space* (2016) 68:82

Page 10 of 20

Mount St. Helens in 1980 (Hoblitt et al. 1981), or to the hydrovolcanic fine ash deposits summarized by Sheridan and Wohletz (1983). The dataset does not show the typical grain-size characteristics observed in magmatic pyroclastic flow, fall, and surge deposits (Walker 1971).

One noticeable feature is that a large proportion of the fine ash is $<4\phi$ (silt–clay size). A significant amount of fine component was found in the proximal area within 500 m of the vent area. We interpret the multiple peaks in the grain histograms as representing the mixing of two or more populations of grain size of different origins. One population is a spread of fine-grained particles with a peak around 8ϕ, and the others represent the coarser grain sizes around 2, 3, and 0ϕ. These populations can be distinctly separated by multiple Gaussian fittings (e.g., Wohletz et al. 1989) (Fig. 9).

The layers can be clearly identified when the grain-size characteristics are displayed alongside the stratigraphic column (Fig. 10). Generally, the bottom layer (Unit A) has finer M_d and better σ_ϕ, and the layers become coarser and more poorly sorted with elevation. At location (*d*), the middle part of the deposit shows relatively finer M_d and better σ_ϕ; hence, this deposit may be subdivided at this stratigraphic level. The finer M_d and better σ_ϕ indicate a temporal waning of the deposition. The topmost layer (Unit C) again has fine M_d. Unit A is generally finer than Unit B when the M_d scale is used, but when the fraction of finer population (FP) is used, Unit A does not show more fine fractions than Unit B. This feature is common to both locations (*d*, *f*); rather, FP seems to increase with height from Unit A to Unit B.
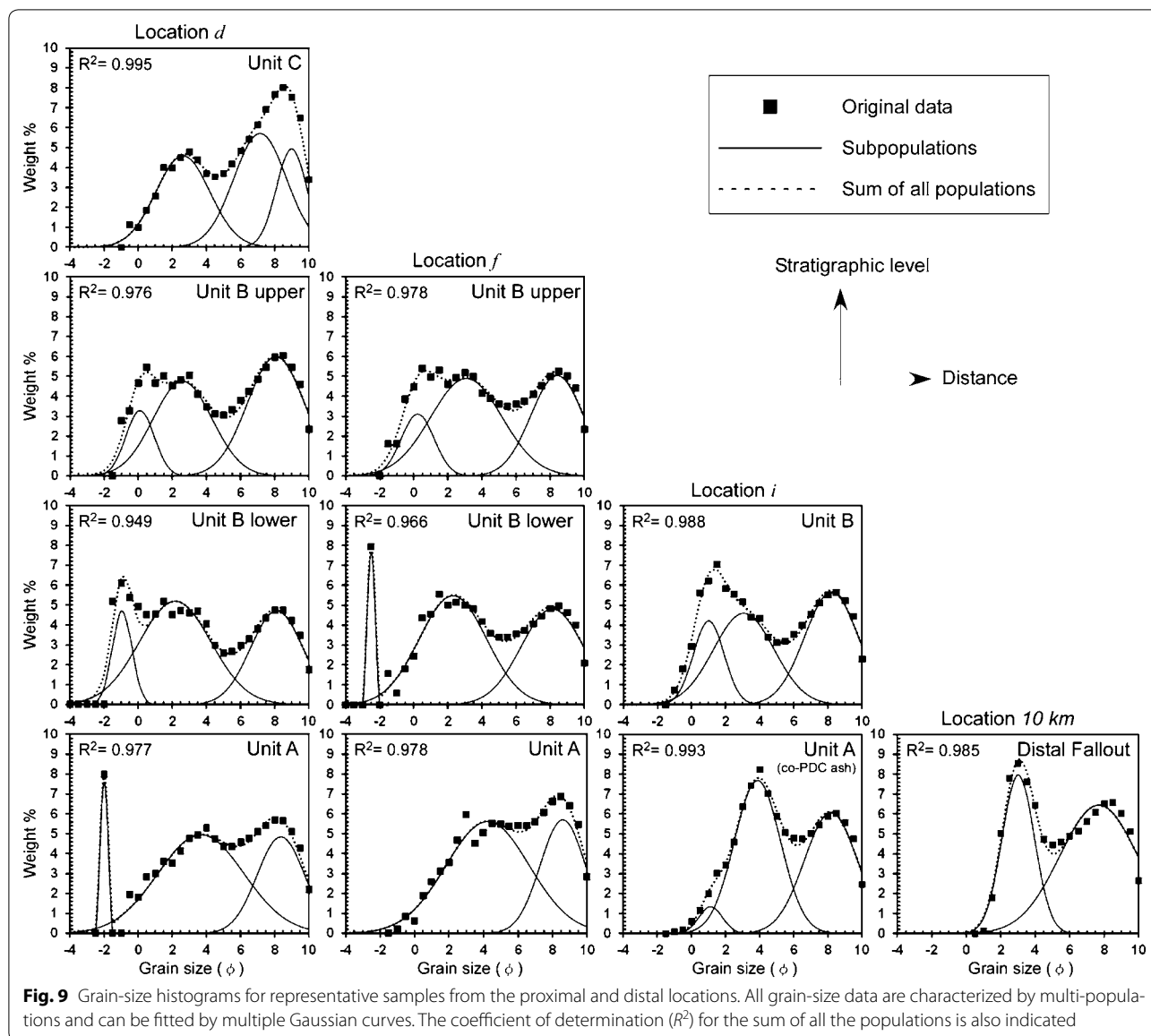
Component analysis

The major components of the eruptive materials are characterized by dense andesitic to dacitic lava with various degrees of alteration. The ash includes shattered crystals derived from the same lava. Hydrothermal minerals such as pyrite are often crystalized on the lava surface. No fresh juvenile components such as pumice or scoria were found in any of the samples. XRD analysis of the very fine components at location (*d*) found hydrothermal minerals such as smectite, kaolinite, pyrite, illite, pyrophyllite, and gypsum with quartz and plagioclase. There were no systematic changes in the components with height. This indicates that these products were derived primarily from fragmentation of country rock and hydrothermally altered material in a hydrothermal reservoir and along the pathways to the surface.

Volume estimation

The products from the Ontake eruption consist of fallout tephra and PDC deposit. In the proximal area, it is difficult to determine each isopach contour of the fallout and the PDC deposits (Fig. 4). However, the PDC deposit layer is much thinner (10–15 % of the entire deposit) than the fallout tephra layer; hence, the contribution of the PDCs to the entire volume is small. This is validated by the volume estimation for PDCs based on other methods in a later section. Here, we calculate the total volume and mass for two extreme cases: case 1 that uses the proximal isopach contours for all the deposits (assuming 100 % fallout deposit) and case 2 that does not use the proximal isopach contours (assuming unknown thickness for proximal fallout and PDC deposits). The deposit density was assumed as ~1000 kg/m^3 in all the calculations. For the two cases, the volume and mass of the fallout deposits were calculated using three methods: (a) integrating multiple exponential segments on a log(mass per unit area) versus log(area) plot (e.g., Froggatt 1982), (b) power-law fitting on log(thickness) versus square root of area plot (Bonadonna and Houghton 2005), and (c) Weibull fitting (Bonadonna and Costa 2012). For methods (a) and (b), different assumptions of tephra thickness at the source yielded maximum and minimum estimates. For the maximum estimates, the tephra thickness or mass at the rim of the vent area (average height) was assumed as 10 m or 10^4 kg/m^2. For the minimum estimates, the tephra thickness or mass was assumed as 3 m or $10^{3.5}$ kg/m^2. The cone height at the vent area was roughly estimated based on aerial photographs in Kaneko et al. (2016). The distal extreme in method (a) was assumed as 10^{-4} kg/m^2 for 10^4 km^2 (minimum) or 10^5 km^2 (maximum). For method (b), the distal extreme was set at 100 km. Both assumptions are based on extrapolation of the measured fallout tephra data. For method (c), fitted curves were integrated between zero and infinity for distance, and the parameter settings followed Bonadonna and Costa (2012) and Maeno et al. (2014).
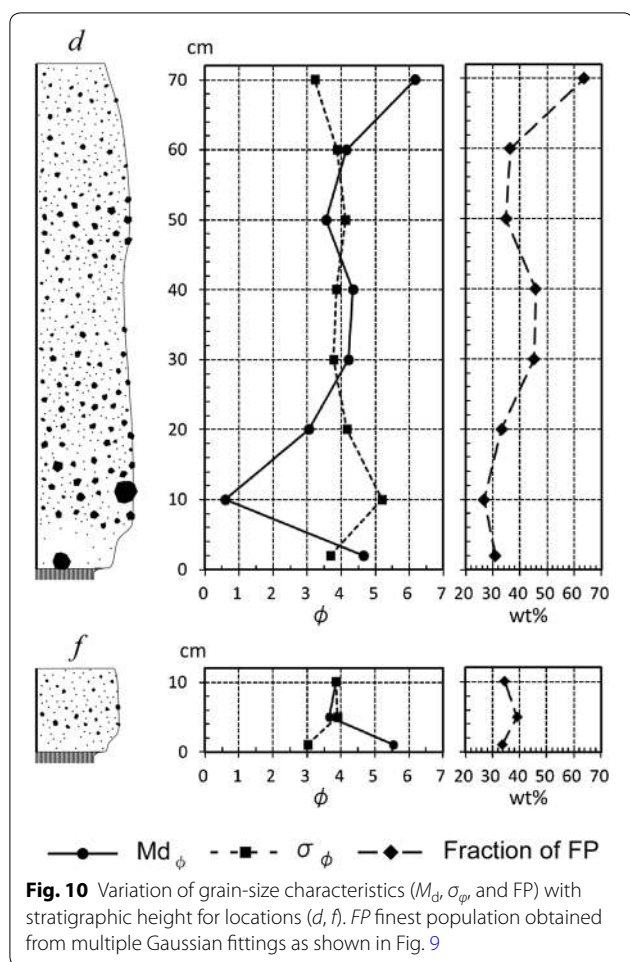
The results are listed in Table 1. In method (a), the total tephra mass was calculated by integrating multiple segments to produce each isomass contour (Fig. 11a). A mass of $0.67–1.3 \times 10^9$ kg, or volume of $0.27–0.52 \times 10^6$ m^3 of dense rock equivalent (DRE), was obtained. In method (b), the estimated tephra volume was $0.28–0.54 \times 10^6$ m^3 in DRE by integrating the power-law curve (Fig. 11b). In method (c), a mass of $0.63–1.4 \times 10^9$ kg, or volume of $0.25–0.56 \times 10^6$ m^3 in DRE, was obtained; however, the sum of the squared relative residuals for the fitting (4.5–5.7) was much higher than those in previous studies (e.g., Maeno et al. 2014), indicating that the estimation of method (c) contains large errors. Note that there are no significant differences between the results of cases 1 and 2, as well as between the different methods (i.e., ~10–15 % error). The results indicate that the determining the precise ratio of fallout to PDC deposits in the proximal area is not of great importance in volume estimation in this case.

Maeno *et al. Earth, Planets and Space* (2016) 68:82

Page 11 of 20

Fig. 9 Grain-size histograms for representative samples from the proximal and distal locations. All grain-size data are characterized by multi-populations and can be fitted by multiple Gaussian curves. The coefficient of determination (R^2) for the sum of all the populations is also indicated

We also estimated the volume of the PDC deposits separately, excluding the deposit in the proximal area (shaded area in Fig. 4b). The PDC deposits extend to the southern and western slopes, but a detailed survey of the deposits was not possible because of difficulty of access. Based on aerial photographs taken by GSI, approximate distributions of the PDCs were drawn. The surface of the slopes covered by PDC deposits is whitish or light gray, but the average thickness is seemingly very thin, because colors from underlying leaves and ground surface are partially identifiable. The deposit is unlikely to be more than a few cm thick on average. Assuming a deposit thickness of 1–2 cm, the volume of the PDC lobes on the southern and western slopes is estimated to

be $0.036–0.072 \times 10^6$ m^3. This is a very rough estimate, but not significantly different from the results of a scaling analysis using a depth-averaged model for particle-laden flows on slopes as discussed in a later section.

Finally, the total volume of eruptive deposits is estimated to be $0.7–1.3 \times 10^6$ m^3 ($0.3–0.5 \times 10^6$ m^3 in DRE), indicating that the magnitude of the eruption (*M*) is ~2. Although it is difficult to constrain the volumes of the PDCs that were emplaced in sequence toward the N–NE, our analyses suggest that the contribution of the PDCs to the total volume is <10 %. The estimated fallout deposit volume is similar to that of the phreatic eruption at Ontake in 1979, where the volume was estimated to be $0.95–1.23 \times 10^6$ m^3 ($0.4–0.5 \times 10^6$ m^3 in DRE) by the

Maeno *et al. Earth, Planets and Space* (2016) 68:82

Page 12 of 20

Fig. 10 Variation of grain-size characteristics (M_d, σ_φ, and FP) with stratigraphic height for locations (*d, f*). *FP* finest population obtained from multiple Gaussian fittings as shown in Fig. 9

same methods used for the 2014 eruption and using the tephra data by Kobayashi (1980).

Discussion

Eruption process and formation of PDCs

One of the important features of the eruption at Ontake was the occurrence of PDCs caused by fountain collapse at the initial phase. The process that generates this type of PDCs is different from the process that causes by the collapse of an initially convective eruption plume during a magmatic eruption as observed in plinian eruptions, in which changes in physical parameters such as mass discharge rate, vent radius, or magma water content contribute to the decrease in buoyancy and trigger column collapse (e.g., Woods 1988). The Ontake eruption was phreatic, as eyewitness observations and component analysis suggest that large amounts of external (surface or hydrothermal) water and country rock were involved in the eruption. External water is important to control the dynamics of the phreatic eruption (e.g., Mastin 1995; Yamamoto et al. 1999). When sufficiently large

volumes of water erupt with country rock, the ascending plume can remain cold and rapidly become denser than the atmosphere even when mixing with air decreases the partial pressure of the vapor and vaporizes some of the water. As a result, fountain collapse may occur, and the relatively cold PDCs can spread with multiple lobes from the collapsing plume, as shown in Figs. 2 and 4 and recorded in direct observations of past phreatic eruptions (e.g., Heiken et al. 1980). Although such PDCs do not become buoyant, it is possible for a fraction of the finer particles to rise from the flow as a buoyant co-PDC lift-off plume (Fig. 2). This mechanism may have generated the PDCs during the initial phase of the Ontake eruption (0–6 min in Fig. 12).

To trigger such a phreatic eruption, a sealed, pressurized hydrothermal reservoir may be required at a certain level above a magmatic heat source as generally inferred from seismic data and component analysis (e.g., Feuillard et al. 1983; Boudon et al. 1998). The study by Nakamichi et al. (2009) of a VLP event at the Ontake volcano indicated a presence of gas flow–solid interaction in the hydrothermal system beneath the volcano. Maeda et al. (2015) also analyzed a VLP event that accompanied the 2014 eruption and revealed that a hydrothermal crack opened when gas ascended from a depth of 0.3–1 km to the surface immediately before the eruption. Thus, a pressurized reservoir may exist at some depth below the vent. When country rock overlying a gas reservoir with local equilibrium between gas and fluid (or water) is suddenly disrupted, pressurized material is rapidly discharged, as in the proposed mechanism of explosion caused by the interaction between hot lava and external water (e.g., Taniguchi 1996). The downward propagation of the expansion wave superheats the water and triggers its explosive vaporization. The country rock is then broken by the impact of the rapid release of the pressurized mixture of vapor and fragmented country rock, resulting in an intense explosion of the non-juvenile material. Numerous ballistic ejecta accompanied with PDCs probably originate from this vent-opening phase when the pressurized mixture is released (Fig. 12). Multiple PDCs (lobes) observed by eyewitnesses emerged and were deposited around the summit area during the initial phase (Figs. 2, 4), indicating that the initial plume was not buoyant enough and repeatedly partially collapsed in different directions. Eventually, the plume height increased and reached 10 km a.s.l. at 12:10 (Sato et al. 2015). The observations suggest that the main plume and/or co-PDC liftoff plumes became buoyant and continued to develop after the initial fountain collapse.

On mixing with air during vent development, the partial pressure of the vapor decreases and some of the water

Maeno *et al. Earth, Planets and Space* (2016) 68:82

Page 13 of 20

Table 1 Estimated volume and mass of Ontake eruption on 27 September 2014

Event date	Method[a]	Case[b]	Volume[c] ($\times 10^6$ m^3)	Mass ($\times 10^9$ kg)
Fallout deposit and proximal pyroclastic density current deposit				
27 September	a	1	0.77–1.1 (0.31–0.46)	0.77–1.1
27 September	a	2	0.67–1.3 (0.27–0.52)	0.67–1.3
27 September	b	1	0.70–1.2 (0.28–0.49)	0.70–1.2
27 September	b	2	0.77–1.4 (0.31–0.54)	0.77–1.4
27 September	c	1	0.63–1.4 (0.25–0.56)	0.63–1.4
27 September	c	2	0.74–1.2 (0.30–0.48)	0.74–1.2
Event date	**Method[d]**		**Volume[c] ($\times 10^6$ m^3)**	**Mass ($\times 10^9$ kg)**
Pyroclastic density current deposit in S and W slopes				
27 September	d	Max	0.072 (0.029)	0.072
27 September	d	Min	0.036 (0.015)	0.036
27 September	e	Max	0.03 (0.01)	0.03
27 September	e	Min	0.005 (0.002)	0.005

[a] Method for fallout: (a) integrating log[mass per unit area (kg/m^2)] versus log[area (m^2)], (b) exponential fitting for log[thickness (m)] versus [area (m^2)]$^{1/2}$, (c) Weibull fitting for log[mass per unit area (kg/m^2)] versus [area (m^2)]$^{1/2}$

[b] Case: Cases 1 and 2 represent calculations that include and exclude proximal isopach data, respectively

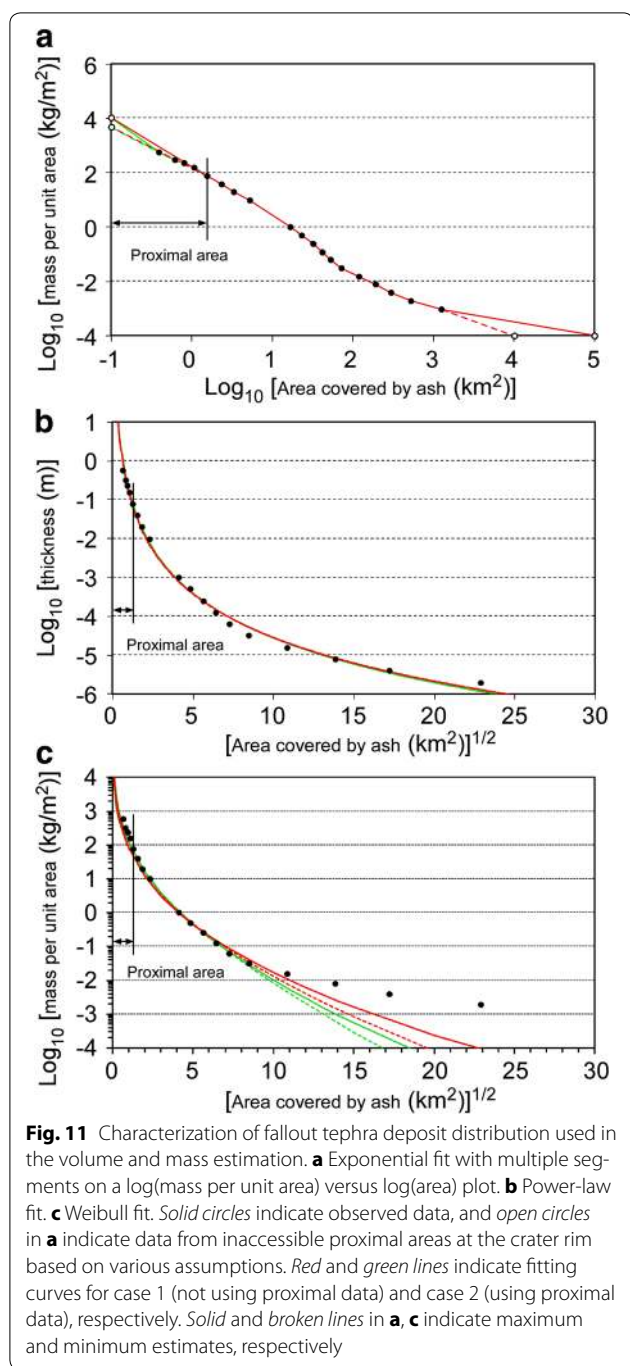[c] Volume in parentheses is DRE (dense rock equivalence) value

[d] Method for PDC: (d) 2 cm and 1 cm in average thickness were assumed for maximum and minimum cases, respectively, (e) Scaling analyses using a depth-averaged gravity flow model

vaporizes. As air continues to be entrained, the temperature and density of the mixture can decrease as proposed for phreatomagmatic eruptions by Koyaguchi and Woods (1996). This process may be effective after the initial PDC phase and cause a plume development reaching 10 km a.s.l. (6–25 min in Fig. 12). As more cold air is added to the mixture by turbulence in the rising plume, the decrease in temperature begins to dominate the decrease in the partial pressure of the vapor. This leads to condensation of the vapor and the formation of aggregates of ash particles in the moist plume. Along with vigorous fallout of wet aggregates and lapillus from the spreading plume, ballistics is continuously ejected as the vent develops. Near the summit area, down currents from the partially collapsing column may also generate minor dilute PDCs. The vertical collapsing flow has relatively high particle concentration and high sedimentation rate, resulting in the formation of a massive poorly sorted deposit, which can be transformed into a lateral dilute traction–suspension current, as observed in large-scale laboratory experiments using cold pyroclastic materials (e.g., Sulpizio et al. 2014). Both sedimentation processes (the direct fallout from a spreading plume in the atmosphere and the down current from a partial column collapse) are plausible near the vent area, although it is difficult to distinguish these processes based only on the deposit data from the limited outcrops. This stage results in the formation of extremely poorly sorted deposits in the proximal area (Unit B). It is likely that this phase caused severe injuries to people and

major damage to buildings around the summit area. The condensation effect was probably significant in the later phase of the eruption and in the distal area and led to the formation of wet aggregates (25 min in Fig. 12). Unit C corresponds to the declining stage that is characterized by the production of wet ash fall.

The effect of particle aggregation on the deposit characteristics

The grain-size distribution of the deposits reflects the transport process. Both the proximal and distal samples show populations of very fine ash particles with an $8 - \phi$ peak (FP in Fig. 9), suggesting that the fine ash was transported as aggregates. The proximal deposits are generally massive and structureless, but are also characterized by ash accretion textures at some locations. Aggregate particles were also observed in distal tephra fallout with similar bulk grain-size characteristics to those of the accretionary lapilli from the Mount St. Helens eruption and hydrovolcanic fine ash deposits (Fig. 8, Hoblitt et al. 1981; Sheridan and Wohletz 1983). FP with an $8 - \phi$ peak was also observed in a deposit from a low-temperature, dilute PDC from a phreatic eruption at Miyakejima in 2000 (Nakada et al. 2005). It is difficult to set constraints on the size distribution of the aggregate of the Ontake eruption; however, the apparent size distribution of the falling particles must be better sorted in a spreading plume. For the proximal deposit, the existence of FP also indicates the effect of aggregation, because the settling
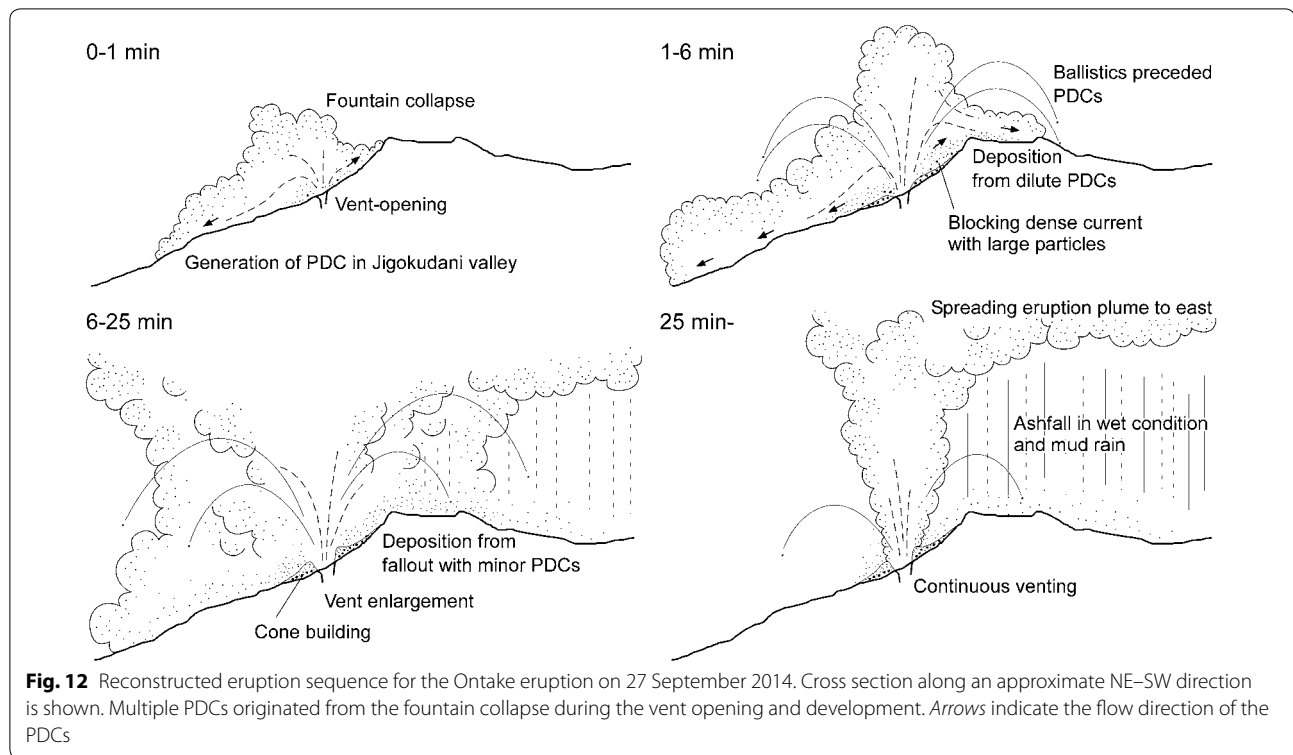
Maeno *et al. Earth, Planets and Space* (2016) 68:82

Page 14 of 20

Fig. 11 Characterization of fallout tephra deposit distribution used in the volume and mass estimation. **a** Exponential fit with multiple segments on a log(mass per unit area) versus log(area) plot. **b** Power-law fit. **c** Weibull fit. *Solid circles* indicate observed data, and *open circles* in **a** indicate data from inaccessible proximal areas at the crater rim based on various assumptions. *Red* and *green lines* indicate fitting curves for case 1 (not using proximal data) and case 2 (using proximal data), respectively. *Solid* and *broken lines* in **a**, **c** indicate maximum and minimum estimates, respectively

velocity of such very fine ash particles is too slow (orders of mm/s or less) to explain the duration of the deposition observed at the study site (Fig. 3).

Witness reports suggest that the depositional condition was relatively dry at the initial phase. Relatively dry conditions can give rise to dry aggregates such as loosely bound particle clusters, characterized by low densities and irregular morphologies (e.g., Sorem 1982). Moisture,

electrostatic attraction, or mechanical interlocking may play a role in the formation of such dry aggregates (Carey and Sigurdsson 1982). With time, water may arise from the condensation of the water vapor directly onto the ash particles in the eruption plume, or from liquid drops ejected with the rock fragments. The growth of wet aggregates depends critically on the ability of the dynamics of these liquid bridges that dissipate the kinetic energy of particle collisions and promote the capture of finer particles (Iveson and Litster 1998). In the later phases of the Ontake eruption, the products changed to show a feature of wet deposition as exemplified by the mud rain. When water is present, the mixture becomes oversaturated and the aggregates collapse into structureless slurry or mud rain (e.g., Van Eaton et al. 2012) rather than form individual solid spherical particles such as accretionary lapilli. It is unlikely that accumulation of slurry generates distinct textures; however, the grain-size characteristic of the grains composing the aggregates may be reflected in the entire deposit characteristics as FP.

Sedimentation from PDCs near the summit
The source of the PDCs that spread west and northeast of the summit during the initial eruption phase was located 200–300 m above the vent area. The steep slope of the Jigokudani valley may have blocked the dense flow containing large particles (Fig. 12) and favored flow separation of the finer particles (e.g., Fisher 1990; Komorowski et al. 2013). Thus, the PDC deposits near the summit are thought to have been derived from finer particles transported by gravity-driven turbulent suspension currents. These currents may have been defected upward by the steep slope and propagated upward until they overflowed the valley rim, or were directly generated from a collapsing plume. The particles may settle directly from the turbulent suspension state with little or no traction, probably owing to their slow speed, forming an unstratified bed in the proximal area, as evidenced by the thin massive fine-grained facies of Unit A. The depositional process of Unit A is comparable to the direct fallout from the dilute PDCs (Branny and Kokelaar 2002; Surpizio and Dellino 2008), where particles are generally supported by fluid turbulence but their velocity is generally too low to create traction along the deposit surface. It is difficult to determine the exact duration of each PDC, but video footage that captured a PDC in Jigokudani and sequential photographs taken from Ninoike suggest that the initial phase lasted 3–6 min. At the summit area, the bottom layer (Unit A) is interpreted as a product from the body of the dilute PDCs. The thickness of Unit A around the summit area is 3–5 cm. Considering the duration, the sedimentation rate of the PDC that spread NE–NW is estimated to be ~1 cm per min in the summit area.

Maeno *et al. Earth, Planets and Space* (2016) 68:82

Page 15 of 20

Fig. 12 Reconstructed eruption sequence for the Ontake eruption on 27 September 2014. Cross section along an approximate NE–SW direction is shown. Multiple PDCs originated from the fountain collapse during the vent opening and development. *Arrows* indicate the flow direction of the PDCs

The grain-size distribution of the deposits has a few peaks, with the main component around 4ϕ (~60 μm) (Fig. 9); however, the falling particles may be larger because of aggregation, with a higher settling velocity. Carey and Sigurdsson (1982) studied the 1980 eruption of Mount St. Helens and found that all tephra particles $<4\phi$ in diameter fell as dry aggregates several hundred microns in diameter with a settling velocity of 0.35 m/s. Lane et al. (1993) demonstrated that the falling aggregates can be modeled as single particles using a reduced aggregate density dependent on the porosity, and deducing a relationship between the particle size and the settling velocity. Considering these studies, we estimate the size of a single particle or aggregate that would settle in dry conditions in the initial phase of the Ontake eruption as 2–4ϕ. Assuming sedimentation from a turbulent suspension current for a period Δt (s), the thickness of the deposit T (m) would be $\rho_p w C_0 \Delta t / \rho_s$ where ρ_p is the density of the particle (2500 kg/m^3), w is the particle settling velocity (m/s), C_0 is the volume fraction of the particles, and ρ_s is the density of the dry deposit (~1000 kg/m^3). The particle settling velocity can be determined from Lane et al. (1993). Using these parameters, the relationship between the sedimentation rate ($s = T/\Delta t$) and C_0 for each particle size can be correlated. As a result, C_0 is calculated as 2×10^{-4} for 2ϕ and 2×10^{-3} for 4ϕ, in which the aggregate porosity was assumed to be 0.4–0.8

(Lane et al. 1993). This result suggests that the volume fraction of the particles of the initial PDCs around the summit area was approximately 10^{-4}–10^{-3}.

Estimation of PDC parameters

The major PDC lobes extend in at least three (SW, NW, and NE) directions (Fig. 4a). At the Jigokudani valley (SW direction), the PDC travelled ~2.4 km down a slope of ~22°. At the western side of Ichinoike (NW direction), the PDC ran ~1.5 km down a slope of ~18° from an altitude of ~2900 m. At the northeastern side (NE direction), the PDC ascended above the Kengamine Peak and overflowed ~600 m from the highest point down the slope of ~12° (Figs. 4, 5). Here, we refer to these PDC lobes as lobe 1, 2, and 3, respectively (Fig. 13a). Although multiple PDCs are thought to have occurred at the summit area, only the PDC with the estimated maximum runout distance in each direction in the initial phase is considered. Lobe 1 was probably not significantly affected by the topographic barrier near the source (Jigokudani valley) as were lobes 2 and 3; thus, the transport and depositional process of lobe 1 may differ from those of lobes 2 and 3. However, here we assume that all the PDC lobes generated by the column collapse are characterized by a similar flow nature.

The PDCs were gravity-driven flows owing to the turbulent suspension of the fine particles. The PDC speed
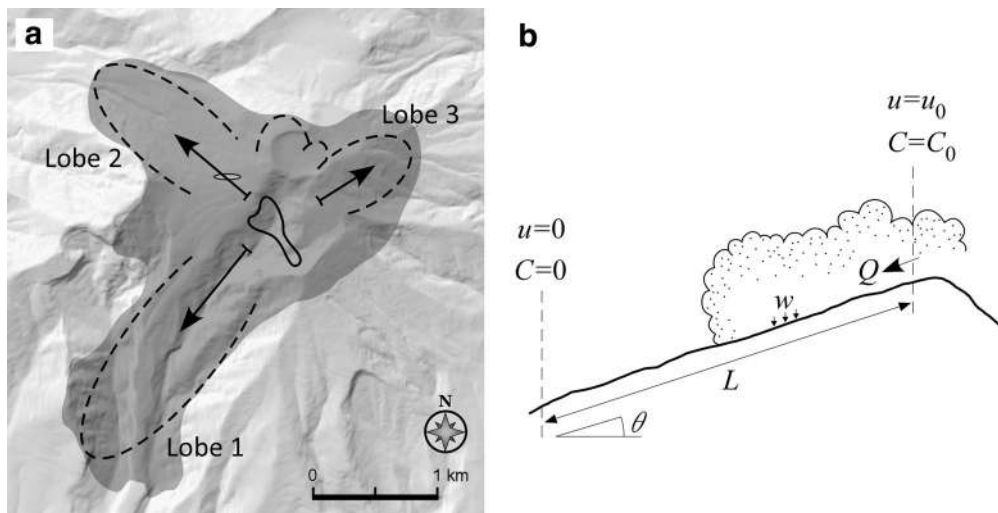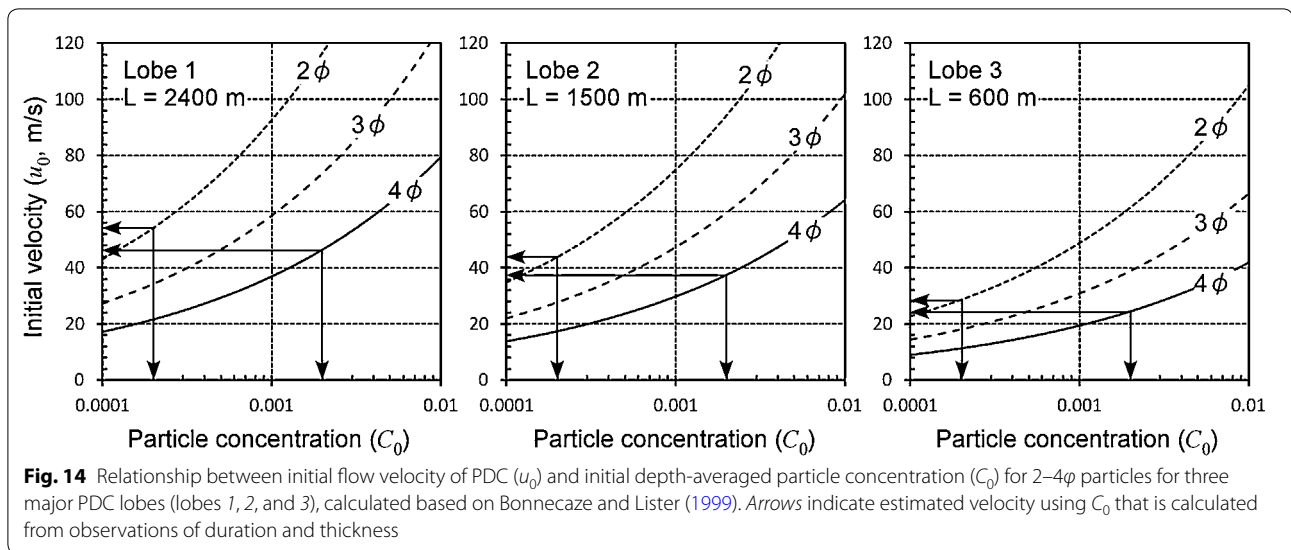
Maeno *et al. Earth, Planets and Space* (2016) 68:82

Page 16 of 20

Fig. 13 a PDC lobes used to estimate the initial condition. **b** Physical parameters used in the model of Bonnecaze and Lister (1999), in which a depth-averaged flow is assumed. *Q* discharge rate, *C* particle concentration, *u* velocity of the PDC, *w* settling velocity of particle, *L* runout distance, *θ* slope angle. The subscript 0 denotes initial values

of lobes 1, 2, and 3 that would achieve runout distances of 2400, 1500, and 600 m in each direction, respectively, can be roughly estimated based on geological data and a scaling analysis using a depth-averaged model of particle-driven gravity currents down slopes (Bonnecaze and Lister 1999). The model considers a turbulent suspension current flowing from a source with a constant flux of fluid down a slope tilted at an angle θ to the horizontal (Fig. 13b). It also assumes that the turbulence keeps the particles well mixed vertically over the current thickness and that the particles leave the current at the base. A scaling analysis can deduce the runout length L as a function of the initial particle concentration C_0, mass flux Q, settling velocity of particle w, and slope angle θ, as follows: $L \approx k(C_0 Q^6/w^8)^{1/11}$, where k is a constant that accounts for the effects of slope angle and gravitational acceleration. The initial flow velocity u_0 is also estimated from the scaling analysis of Bonnecaze and Lister (1999) and is proportional to $C_0^{1/2}$. The source locations were assumed to be 200–300 m from the vent (Fig. 13a). They correspond to the highest point in each direction for lobes 2 and 3, where turbulent dilute PDCs may be generated. For lobe 1, 200 m was assumed, which is the same distance as lobe 2. The relationships between the initial velocity u_0 and the depth-averaged particle concentration C_0 for each PDC lobe are shown in Fig. 14. For lobe 3, using the estimated particle concentration at the proximal region (2×10^{-4} for 2ϕ and 2×10^{-3} for 4ϕ), u_0 is estimated to be 24–28 m/s. Assuming the same particle concentration and particle-size characteristics for lobes 1 and 2, u_0 is estimated to be 46–56 and 38–44 m/s,

respectively. Yamamoto (2014) estimated the speed of lobe 1 at 8–20 m/s for the latter half of the flow based on video images. Our results are consistent with this estimate because the flow decelerated with time and distance owing to particle settling. If we use 4ϕ as the representative particle size, u_0 takes lower values. These results suggest that the PDCs during the Ontake eruption were relatively slow moving, compared with more energetic non-juvenile eruptions (Yamamoto et al. 1999; Fujinawa et al. 2008; Lube et al. 2014). However, they were similar to the dilute PDC with an average speed of ~25 m/s observed in the phreatic eruption at La Soufriere, Guadeloupe, on 2 October 1976 (Heiken et al. 1980), and were a little faster than the a low-temperature, dilute PDC that had an estimated speed of ~15 m/s near the source in the phreatic eruption at Miyakejima in 2000 (Nakada et al. 2005).

The volume of the PDCs can also be constrained using mass flux and duration. For the case with duration of 360 s and a particle size of 2ϕ, the volume of the deposits (DRE) is estimated to be 7000, 3000, and 900 m^3 for lobes 1, 2, and 3, respectively. If we use a particle size of 4ϕ, or a 1-min duration, the volumes decrease by 1/5. The results imply that the volume of the PDCs in the initial stage is of the order of 10^3–10^4 m^3 (Table 1). The above estimation is based on the assumption of constant particle size inside the PDC; however, if the aggregation is more significant, the volume estimation will change because an increase in particle size owing to aggregation causes an increase in the settling velocity. This also causes a decrease in the particle concentration in the flow in the shorter duration.

Maeno *et al. Earth, Planets and Space* (2016) 68:82

Page 17 of 20

Fig. 14 Relationship between initial flow velocity of PDC (u_0) and initial depth-averaged particle concentration (C_0) for 2–4φ particles for three major PDC lobes (lobes *1*, *2*, and *3*), calculated based on Bonnecaze and Lister (1999). *Arrows* indicate estimated velocity using C_0 that is calculated from observations of duration and thickness

Therefore, to achieve the same runout distance, a higher initial discharge rate or higher particle concentration is required, resulting in a larger volume of deposit.

Origin of proximal deposit

The sizes of the particles transported in turbulent suspension depend on the speed of the current. We obtained the relationship between the speed of the turbulent PDC and the size of the particles in suspension using the turbulent boundary layer theory (Valentine 1987; Dellino et al. 2008). For lobe 3 with an initial velocity of 24–28 m/s, the particle sizes that can be transported by turbulent suspension are estimated to be less than ~1 mm. This is consistent with the fact that Unit A at locations (*d, f, i*) that are characterized by populations finer than 0ϕ (~500 μm) was formed by the initial PDCs. Larger clasts that are a few mm to cm in size are also occasionally contained in Unit A close to the vent area; however, it is unlikely that they were transported by PDCs as they cannot be sustained by the turbulence and settle rapidly. Such relatively larger particles would be transported mainly by fallout from the spreading plume. This also applies to particles deposited in the later stage. The deposit characteristics (the M_d–σ_ϕ plot in Fig. 8) support this idea; they are similar to those of the poorly sorted fallout deposits from phreatic eruptions at Bandai, Adatara, and Mount St. Helens; moreover, there is no solid evidence that larger-scale PDCs were produced in the later phase of the eruption. Although smaller PDCs may have occurred in the later stage, it is difficult to constrain the detailed process based only on data from the deposit.

In the proximal area, the effect of aggregation was probably significant in the later stage. Block- and lapilli-sized clasts were deposited as ballistics or fallout tephra in wet conditions, simultaneously with fine-grained ash (silt–clay component), resulting in the formation of an extremely poorly sorted deposit. The tephra thinning trend in the fallout deposits shows a steep slope in the proximal area (Fig. 15). This characteristic is different from those for similar-sized magmatic eruptions such as vulcanian and dome collapse events (on the order of 10^5 m^3 in DRE volume for Soufriere Hills Volcano; Bonadonna et al. 2002) and indicates that a large volume of material was deposited in the proximal area owing to the wet dispersal condition. A tephra thinning trend similar to the 2014 eruption was observed in the phreatic eruption at Ontake in 1979. These thinning trends of the fallout deposits from the phreatic eruptions at Ontake are similar to those observed at subplinian events (Fig. 15), although it is unclear whether this characteristic is common in other phreatic eruptions.

Concluding remarks

Most of the deposits from the phreatic eruption at Ontake volcano on 27 September 2014 are characterized by massive, extremely poorly sorted, and multimodal grain-size distribution with a large fraction of silt- to clay-sized fine ash component. Based on the deposit facies observed in this study, we can divide the deposit into three major units (Units A, B, and C). Combining geological data with witness observations suggesting that the depositional condition was initially dry but eventually changed to wet, we conclude that Unit A originated from gravity-driven dilute PDCs in the relatively dry, vent-opening phase. Unit B was produced mainly by fallout from a vigorous moist plume during vent development. Unit C was formed by wet ash fall in the declining stage.
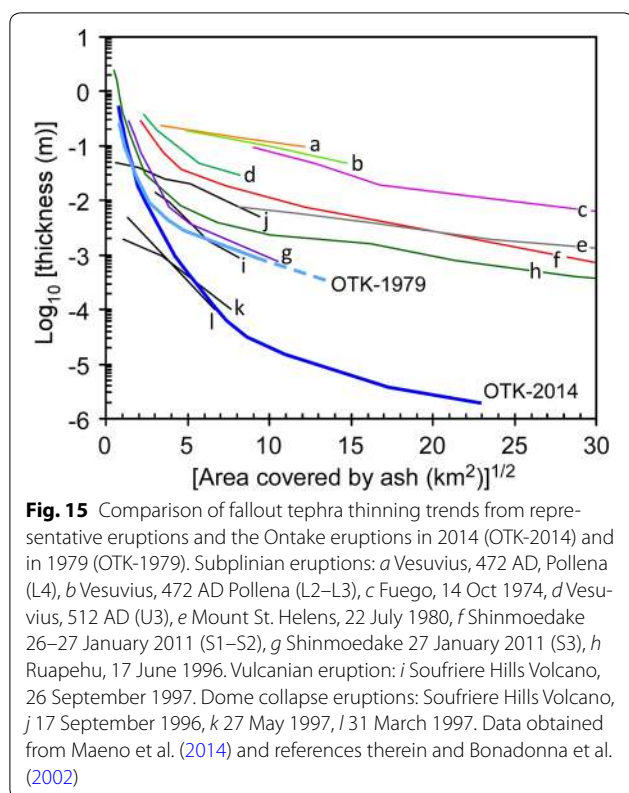
Fig. 15 Comparison of fallout tephra thinning trends from representative eruptions and the Ontake eruptions in 2014 (OTK-2014) and in 1979 (OTK-1979). Subplinian eruptions: *a* Vesuvius, 472 AD, Pollena (L4), *b* Vesuvius, 472 AD Pollena (L2–L3), *c* Fuego, 14 Oct 1974, *d* Vesuvius, 512 AD (U3), *e* Mount St. Helens, 22 July 1980, *f* Shinmoedake 26–27 January 2011 (S1–S2), *g* Shinmoedake 27 January 2011 (S3), *h* Ruapehu, 17 June 1996. Vulcanian eruption: *i* Soufriere Hills Volcano, 26 September 1997. Dome collapse eruptions: Soufriere Hills Volcano, *j* 17 September 1996, *k* 27 May 1997, *l* 31 March 1997. Data obtained from Maeno et al. (2014) and references therein and Bonadonna et al. (2002)

As evidenced in the finest population of the grain-size distribution, aggregate particles were formed throughout the eruption, and the effect of the water in the plume on aggregation increased with time and distance.

The lithofacies and grain-size characteristics of the poorly sorted deposits observed in the proximal area are similar to those of mudflows or fallout tephra from past phreatic events. However, Unit A is certainly derived from PDCs. It is important to understand the similarity of the deposits when we interpret this type of poorly sorted deposit solely based on geological records. Particularly, care must be taken when reconstructing past eruption events and evaluating potential hazards relating to future phreatic eruptions. The Ontake eruption provided an important opportunity to study proximal deposits from a phreatic eruption that provides a complex eruption sequence and reflects the effect of water on the eruption dynamics.

Using geological records, witness observations, and a theoretical approach, the physical parameters of the eruption can be constrained. Based on the deposit thickness, duration, and grain-size data, the particle concentration and initial flow velocity for three PDC lobes in the initial phase were estimated to be 2×10^{-4}–2×10^{-3} and 24–56 m/s, respectively, applying a scaling analysis using a depth-averaged model of turbulent gravity currents flowing down slopes. Further studies may enable to quantitatively evaluate the major factors that caused the many casualties and severe damage to buildings near the eruption source during the Ontake eruption.

Author details
[1] Earthquake Research Institute, The University of Tokyo, 1-1-1, Yayoi, Bunkyo-ku, Tokyo 113-0032, Japan. [2] Geological Survey of Japan, AIST, 1-1-1 Higashi, Tsukuba, Ibaraki 305-8567, Japan. [3] Mount Fuji Research Institute, Yamanashi Prefectural Government, 5597-1 Kenmarubi, Kamiyoshida, Fuji-yoshida, Yamanashi 403-0005, Japan. [4] Faculty of Modern Life, Teikyo Heisei University, 4-21-2, Nakano, Nakano-ku, Tokyo 164-8530, Japan. [5] Institute of Education, Shinshu University, 6-Ro, Nishinagano, Nagano City, Nagano 380-8544, Japan. [6] Graduate School of Environmental and Disaster Research, Tokoha University, Obuchi 325, Fuji City, Shizuoka 417-0801, Japan. [7] National Research Institute for Earth Science and Disaster Resilience, 3-1, Tennodai, Tsukuba, Ibaraki 305-0006, Japan.

References
Barberi F, Bertagnini A, Landi P, Principe C (1992) A review on phreatic eruptions and their precursors. J Volcanol Geotherm Res 52:231–246
Bonadonna C, Costa A (2012) Estimating the volume of tephra deposits: a new simple strategy. Geology 40:415–418
Bonadonna C, Houghton BF (2005) Total grain-size distribution and volume of tephra-fall deposit. Bull Volcanol 67:441–456
Bonadonna C, Mayberry GC, Calder ES, Sparks RSJ, Choux C, Jackson P, Lejeune AM, Loughlin SC, Norton GE, Rose WI, Ryan G, Young SR (2002) Tephra fallout in the eruption of Soufriere Hills Volcano, Montserrat. In: Druitt TH, Kokelaar BP (eds) The eruption of Soufriere Hills Volcano, Montserrat, from 1995 to 1999, vol 21. Memoirs of the Geological Society of London, London, pp 483–516
Bonnecaze RT, Lister JR (1999) Particle-driven gravity currents down planar slopes. J Fluid Mech 390:75–91
Boudon G, Villemant B, Komorowski J-C, Ildefonse P, Semet MP (1998) The hydrothermal system at Soufriere Hills volcano, Montserrat (West Indies): characterization and role in the on-going eruption. Geophys Res Lett 25(19):3693–3696
Branny MJ, Kokelaar P (2002) Pyroclastic density currents and the sedimentation of ignimbrites. Geol Soc Lond Mem 27:1–143
Browne PRL, Lawless JV (2001) Characteristics of hydrothermal eruptions, with examples from New Zealand and elsewhere. Earth Sci Rev 52:299–331

Maeno *et al. Earth, Planets and Space* (2016) 68:82

Page 19 of 20

Carey SN, Sigurdsson H (1982) Influence of particle aggregation on deposition of distal tephra from the May 18, 1980 eruption of Mount St. Helens' volcano. J Geophys Res 87(B8):7061–7072

Dellino P, Mele D, Sulpizio R, La Volpe L, Braia G (2008) A method for the calculation of the impact parameters of dilute pyroclastic density currents based on deposits particle characteristics. J Geophys Res 113:B07206

Feuillard M, Allegre CJ, Brandeis G, Caulon R, Le Mouel JL, Mercier JC, Pozzi JP, Semet MP (1983) The 1975–1977 crisis of La Soufrière de Guadeloupe (F.W.I): a still-born magmatic eruption. J Volcanol Geotherm Res 16:317–334

Fisher RV (1990) Transport and deposition of a pyroclastic surge across an area of high relief—the 18 May 1980 eruption of Mount St. Helens, Washington. Geol Soc Am Bull 102:1038–1054

Froggatt PC (1982) Review of methods of estimating rhyolitic tephra volumes; applications to the Taupo Volcanic Zone, New Zealand. J Volcanol Geotherm Res 14:301–318

Fujinawa A, Ban M, Ohba T, Kontani K, Miura K (2008) Characterization of low-temperature pyroclastic surges that occurred in the northern Japan arc during the late 19th century. J Volcanol Geotherm Res 178:113–130

Geospatial Information Authority of Japan (2014) Response to the volcanic activity at Ontake volcano. http://www.gsj.go.jp/BOUSAI/h26-ontake-index.html. Accessed 5 Oct 2015

Hedenquist JW, Henley RW (1985) Hydrothermal eruptions in the Waiotapu geothermal system. Econ Geol 80:1640–1688

Heiken G, Crowe B, McGetchin T, West F, Eichelberger J, Bartram D, Peterson R, Wohletz K (1980) Phreatic eruption clouds: the activity of la Soufrière de Guadeloupe, F.W.I., August–October, 1976. Bull Volcanol 43:383–395

Hincks TK, Komorowski J-C, Sparks RSJ, Aspinall WP (2014) Retrospective analysis of uncertain eruption precursors at La Soufrière volcano, Guadeloupe, 1975–1977: volcanic hazard assessment using a Bayesian belief network approach. J Appl Volcanol 3:3

Hoblitt RP, Miller DC, Vallance JE (1981) Origin and stratigraphy of the deposits produced by the May 18 directed blast. In: Lipman PW, Mullineaux DR (eds) The 1980 eruptions of Mount St. Helens, Washington. US Geological Survey Prof. Rep. No. 1250. US Geological Survey, Washington, pp 401–419

Inman DL (1952) Measures of describing the size distribution of sediments. J Sediment Petrol 22:125–145

Iveson SM, Litster JD (1998) Growth regime map for liquid-bound granules. Am Inst Chem Eng J 44:1510–1518

Japan Meteorological Agency (1991) Ontake volcano. Bull Volcanol Soc Jpn 36:385 **(in Japanese)**

Japan Meteorological Agency (2014) A monthly report on volcanic activity at Ontake. http://www.data.jma.go.jp/svd/vois/data/tokyo/STOCK/monthly_v-act_doc/tokyo/14m09/312_14m09.pdf. Accessed on 5 Oct 2015 **(in Japanese)**

Kaneko T, Maeno F, Nakada S (2016) 2014 Mount Ontake eruption: characteristics of the phreatic eruption as inferred from aerial observations. Earth Planets Space 68:72. doi:10.1186/s40623-016-0452-y

Kato A, Terakawa T, Yamanaka Y, Maeda Y, Horikawa S, Matsuhiro K, Okuda T (2015) Preparatory and precursory processes leading up to the 2014 phreatic eruption of Mount Ontake, Japan. Earth Planets Space 67:111

Kobayashi T (1980) The eruptive activity at Ontake volcano in 1979. Report for a grant from the Japanese Ministry of Education, Science and Culture (PI: Aoki H), pp 4–12 **(in Japanese)**

Komorowski J-C, Jenkins S, Baxter PJ, Picquout A, Lavigne F, Charbonnier S, Gertisser R, Preece K, Cholik N, Budi-Santoso A (2013) Paroxysmal dome explosion during the Merapi 2010 eruption: processes and facies relationships of associated high-energy pyroclastic density currents. J Volcanol Geotherm Res 261:260–294

Koyaguchi T, Woods AW (1996) On the formation of eruption columns following explosive mixing of magma and surface-water. J Geophys Res 101(B3):5561–5574

Lane SJ, Gilbert JS, Hilton M (1993) The aerodynamic behaviour of volcanic aggregates. Bull Volcanol 55:481–488

Lube G, Breard ECP, Cronin SJ, Procter JN, Brenna M, Moebis A, Pardo N, Stewart RB, Jolly A, Fournier N (2014) Dynamics of surges generated by hydrothermal blasts during the 6 August 2012 Te Maari eruption, Mt. Tongariro, New Zealand. J Volcanol Geotherm Res 286:348–366

Maeda Y, Kato A, Terakawa T, Yamanaka Y, Horikawa S, Matsuhiro K, Okuda T (2015) Source mechanism of a VLP event immediately before the 2014 eruption of Mt. Ontake, Japan. Earth Planets Space 67:187

Maeno F, Nagai M, Nakada S, Burden RE, Engwell S, Suzuki Y, Kaneko T (2014) Constraining tephra dispersion and deposition from three subplinian explosions in 2011 at Shinmoedake volcano, Kyushu, Japan. Bull Volcanol 76:823. doi:10.1007/s00445-014-0823-9

Mastin LG (1995) Thermodynamics of gas and steam-blast eruptions. Bull Volcanol 57:85–98

Nakada S, Nagai M, Kaneko T, Nozawa A, Suzuki-Kamata K (2005) Chronology and products of the 2000 eruption of Miyakejima volcano, Japan. Bull Volcanol 67:205–218

Nakamichi H, Kumagai H, Nakano M, Okubo M, Kimata F, Ito Y, Obara K (2009) Source mechanism of a very-long-period event at Mt Ontake, central Japan: response of a hydrothermal system to magma intrusion beneath the summit. J Volcanol Geotherm Res 187:167–177

Ohba T, Taniguchi H, Miyamoto T, Hayashi S, Hasenaka T (2007) Mud plumbing system of an isolated phreatic eruption at Akita Yakeyama volcano, northern Honshu, Japan. J Volcanol Geotherm Res 161:35–46

Oikawa T (2008) Reinvestigation of the historical eruption and fumarolic activity records at Ontake Volcano, central Japan. Misunderstanding reports about the 774 AD and 1892 AD eruptions. Bull Geol Surv Jpn 59:203–210 **(in Japanese with English abstract)**

Oikawa T, Yamaoka K, Yoshimoto M, Nakada S, Takeshita Y, Maeno F, Ishizuka Y, Komori J, Shimano T, Nakano S (2015) The 2014 eruption of Ontake volcano, Central Japan. Bull Volcanol Soci Jpn 60:411–415

Oikawa T, Yoshimoto M, Nakada S, Maeno F, Komori J, Shimano T, Ishizuka Y, Takeshita Y, Ishimine Y (2016) Reconstruction of the 2014 eruption sequence of Ontake volcano (Ontake-san) from recorded images and interviews. Earth Planets Space. doi:10.1186/s40623-016-0458-5

Sato E, Shimbori T, Fukui K, Ishii K, Takagi A (2015) The eruption cloud echo from Mt. Ontake on September 27, 2014, observed by weather radar network. Rep. Coordinating Committee for Prediction of Volcanic Eruptions No. 119, Japan Meteorological Agency, Tokyo **(in press) (in Japanese)**

Sheridan MF, Wohletz KH (1983) Hydrovolcanism: basic considerations and review. J Volcanol Geotherm Res 17:1–29

Sorem RK (1982) Volcanic ash clusters: tephra rafts and scavengers. J Vocanol Geotherm Res 13:63–71

Sulpizio R, Dellino P, Doronzo DM, Sarocchi D (2014) Pyroclastic density currents: state of the art and perspectives. J Volcanol Geotherm Res 283:36–65

Surpizio R, Dellino P (2008) Sedimentology, depositional mechanisms and pulsating behaviour of pyroclastic density currents. In: Gottsmann J, Marti J (eds) Caldera volcanism, developments in volcanology, vol 10. Elsevier, Amsterdam, pp 57–96

Suzuki Y, Nagai M, Maeno F, Yasuda A, Hokanishi N, Shimano T, Ichihara M, Kaneko T, Nakada S (2013) Precursory activity and evolution of the 2011 eruption of Shinmoe-dake in Kirishima volcano—insights from ash samples. Earth Planets Space 65:591–607

Taniguchi H (1996) Mechanism of a phreatomagmatic explosion due to the interaction between hot rhyolitic lava flow and external water. Mem Geol Soc Jpn 46:149–162 **(in Japanese with English abstract)**

The Joint Research Team for Ash Fall from the Ontake 2014 Eruption (2015) Ash fall distribution of Sep. 27 2014 in Ontake volcano. Rep. Coordinating Committee for Prediction of Volcanic Eruptions No. 119, Japan Meteorological Agency, Tokyo **(in press) (in Japanese)**

The Shinano Mainichi Shimbun (2015) Inspection of the Ontake eruption. The Shinano Mainichi Shinbun, Nagano, pp 1–263 **(in Japanese)**

Tsunematsu K, Ishimine Y, Kaneko T, Yoshimoto M, Fujii T, Yamaoka K (2016) An estimate of ballistic block landing energy for the 2014 eruption of Ontake volcano. Earth Planets Space. doi:10.1186/s40623-016-0463-8

Valentine GA (1987) Stratified flow in pyroclastic surges. Bull Volcanol 49:616–630

Van Eaton AR, Muirhead JD, Wilson CJN, Cimarelli C (2012) Growth of volcanic ash aggregates in the presence of liquid water and ice: an experimental approach. Bull Volcanol 74:1963–1984

Walker GPL (1971) Grain-size characteristics of pyroclastic deposit. J Geol 79:696–714

Wohletz K, Heiken G (1992) Volcanology and geothermal energy. University of California Press, Berkeley, p 432

Maeno *et al. Earth, Planets and Space* (2016) 68:82

Page 20 of 20

Wohletz K, Sheridan MF, Brown WK (1989) Particle size distribution and the sequential fragmentation/transport theory applied to volcanic ash. J Geophys Res 94(B11):15703–15721

Woods AW (1988) The fluid dynamics and thermodynamics of eruptions columns. Bull Volcanol 50:169–193

Yamamoto T (2014) The pyroclastic density currents generated by the September 27, 2014 phreatic eruption of Ontake volcano, Japan. Bull Geol Surv Jpn 65:117–127 **(in Japanese with English abstract)**

Yamamoto T, Nakamura Y, Glicken H (1999) Pyroclastic density current from the 1888 phreatic eruption of Bandai volcano, NE Japan. J Volcanol Geotherm Res 90:191–207

Young SR, Sparks RSJ, Aspinall WP, Lynch LL, Miller AD, Robertson REA, Shepherd JB (1998) Overview of the eruption of Soufriere Hills volcano, Montserrat, 18 July 1995–December 1997. Geophys Res Lett 25(18):3389–3392